Inorganic Chemistry

Article

pubs.acs.org/IC

Design of a Family of Ln_3 Triangles with the HAT Ligand (1,4,5,8,9,12-Hexaazatriphenylene): Single-Molecule Magnetism

Ismael F. Díaz-Ortega,[†] Juan Manuel Herrera,*[,†] Tulika Gupta,[‡] Gopalan Rajaraman,*[,‡] Hiroyuki Nojiri,*[,§] and Enrique Colacio*[,†]

[†]Departamento de Química Inorgánica, Facultad de Ciencias, Universidad de Granada, Avda. Fuentenueva s/n, 18071 Granada, Spain

[‡]Department of Chemistry, Indian Institute of Technology Bombay, Powai, Mumbai 400076, India

[§]Institute for Materials Research, Tohoku University, Katahira, Sendai 980-8577, Japan

Supporting Information

ABSTRACT: A series of trinuclear Ln_3 complexes (Ln^{III} = Yb (**1**), Er (**2**), Dy (**3**) and Gd (**4**)) were prepared from the tris-chelate bidentate ligand 1,4,5,8,9,12-hexaazatriphenylene (HAT). **1** and **2** exhibited field-induced single-molecule-magnet (SMM) behavior with estimated U_{eff} values of 21.30 and 13.86 K, respectively. Complex **3** behaved as a SMM even at zero field, and two different thermally assisted relaxation processes were detected with U_{eff} values of 29.6 K (fast relaxation process, FR) and 69 K (slow relaxation process, SR) due to the existence of two magnetically different Dy^{III} centers in the molecule. Ab initio studies reveal that all the Dy^{3+} centers have almost an Ising ground state. The local anisotropy axes are not coplanar but form angles with the Dy3 plane in the range 58−78°. The magnetic interaction between the anisotropic Dy^{3+} ions is antiferromagnetic in nature and very weak in magnitude. However, due to the extreme feebleness of the magnetic interaction with regard to the local excitation energies, the magnetization blockade is most probably of single-ion origin. Calculations support the existence of two relaxation processes, which take place through the first excited state following an Orbach/Raman mechanism. Finally, for complex **4**, the magnetocaloric effect was simulated using the magnetic parameters extracted from the fit of the magnetization and susceptibility data and demonstrated that the simulated $-\Delta S_m$ values were almost coincident with those extracted from the integration of the field dependence of the magnetization. The simulated MCE value at 2 K and 5 T (20.46 J kg^{-1} K^{-1}) makes complex **4** an attractive candidate for cryogenic magnetization.

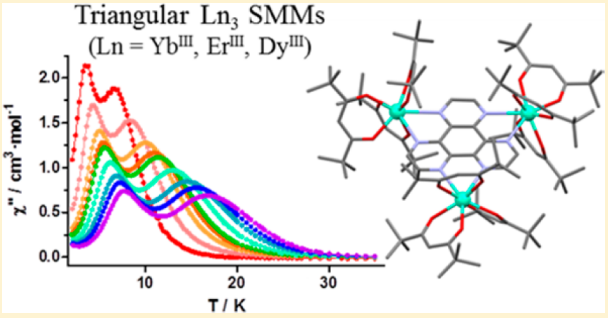

INTRODUCTION

Since the discovery in the early 1990s that molecules can behave as superparamagnets exhibiting slow relaxation of the magnetization and magnetic hysteresis below a certain temperature (T_B), many efforts have been devoted to determine the parameters that govern this fascinating behavior.[1] The origin of single-molecule-magnet (SMM) behavior is the existence of an energy barrier (U) that prevents the reversal of the magnetization when the external field is removed. To date, the observed energy barriers are rather low and molecules behave as SMMs only at very low temperatures. To increase the energy barrier height and therefore T_B ($T_B \propto U$), systems with large spin ground states (S) and large axial anisotropy (D) are required. For many years, many synthetic efforts were made to prepare magnetically coupled transition-metal clusters of high nuclearity, on the basis of the belief that more efficient single-molecule magnets should possess large S values.[2] This strategy was demonstrated to be fruitless, as polynuclear clusters with large S values featured D values close to 0, dramatically preventing the enhancement of the spin-reversal barrier.[3] Considering a different approach, researchers now have focused their synthetic efforts on maximizing the anisotropy of small and even mononuclear molecules based on metal ions with high-spin ground states. Due to their intrinsic large magnetic anisotropy and large magnetic moment, lanthanides were quickly chosen for the development of this new strategy.[4] In particular, some mono- and dinuclear Dy(III)-based molecules can be considered as cornerstones in the development of this field, as they show slow relaxation of the magnetization with the highest relaxation energy barriers and the highest temperatures at which magnetic hysteresis has been ever observed for SMMs.[5] Efforts to prepare lanthanide clusters with higher nuclearity have allowed the discovery of a new magnetic phenomenon called spin chirality in triangular Dy_3 clusters.[6] In these complexes, the coexistence of SMM behavior and an essentially diamagnetic ground state was observed. This unexpected behavior is due to the noncollinearity of the planar easy anisotropy axis of the Dy^{III} ions.[7] The discovery of this fascinating magnetic behavior has ignited new interest in the

Received: December 13, 2016
Published: May 3, 2017

DOI: 10.1021/acs.inorgchem.6b03031
Inorg. Chem. 2017, 56, 5594−5610

design of new Dy_3 triangles in order to determine how different factors such as the molecular symmetry and the existence of exchange and/or dipole magnetic interactions can influence the toroidal alignment of the local magnetic moments.[8] In addition to triangular Dy_3 clusters, higher-nuclearity Dy_4 and Dy_6 compounds have been reported to exhibit a toroidal magnetic structure.[9] Furthermore, it has also been shown how the existence of hydrogen bonds linking two Dy_3 units can increase the thermal energy barrier or how their antiferromagnetic coupling through paramagnetic Cu(II) complexes led to multiferroic 1D systems.[10] These results point out the potential of triangular Dy_3 units in the design of multifunctional materials. For the preparation of these single-molecule toroids (SMTs), a tight control of the toroidal alignment of the individual Dy(III) magnetic moments is necessary. A possible strategy to exert such control is the use of tris-chelate ligands able to dispose the Dy(III) centers forming a equatorial triangle. A possible candidate for this purpose is the ligand 1,4,5,8,9,12-hexaazatriphenylene (HAT).[11] This is a highly symmetric tris-chelate bidentate ligand that has been previously used to prepare discrete trinuclear species as well as coordination polymers where the ligand was coordinate to three metal centers.[12] Here we report the synthesis, X-ray structure, magnetic properties, and theoretical calculations of the new dysprosium triangle $\{(HAT\text{-}\mu_3)[Dy(tmh)_3]_3\}$, where the Dy(III) centers are connected through the HAT ligand and their coordination sphere is completed by three β-diketonate ligands (tmh = 2,2,6,6-tetramethylheptanoate). Additionally, three isostructural complexes based on Gd(III), Er(III), and Yb(III) ions have been prepared and studied from a structural and magnetic point of view. It should be noted at this point that during the course of this research work the very similar complex $\{(HAN\text{-}\mu_3)[Dy(tmh)_3]_3\}$ (HAN = hexaazatrinaphthylene) has been reported,[13] which represented the first example of a trilanthanide complex of this family (HAT and HAN) of tritopic ligands.

EXPERIMENTAL SECTION

General Procedures. The synthesis of 1,4,5,8,9,12-hexaazatriphenylene (HAT) was carried out as described by Czarnik et al.[11] All others reagents and solvents were purchased from commercial sources and used as received.

Synthesis of $[Ln(tmh)_3(\mu_3\text{-HAT})]$ (Ln^{III} = Yb (1), Er (2), Dy (3) and Gd(4)). These complexes were prepared as follows. Solutions of HAT (0.125 mmol) in a CH_3OH/CH_2Cl_2 mixture (1/1, v/v) and the appropriate $Ln(NO_3)_3{\cdot}6H_2O$ complex (0.375 mmol) in CH_3OH (5 mL) were mixed, resulting in a yellow solution, to which a mixture of Htmh (1.125 mmol) and Et_3N (1.125 mmol) in CH_3OH (5 mL) was added without stirring. The resulting solution was left to stand over a period of 1−2 h, after which a good crop of orange crystals was obtained. The crystals were filtered, washed with methanol, and air-dried. Analytical data for these complexes are collected in Table S1 and Figure S1 in the Supporting Information.

X-ray Crystallography. Suitable crystals of complexes **1**−**3** were mounted on a Bruker D8 Venture instrument (Mo Kα radiation, λ = 0.71073 Å, Photon 100 CMOS detector). Details of the crystal data and data collection and refinement parameters are reported in Table S2 in the Supporting Information. Once the data were processed (raw data integration, merging of equivalent reflections, and empirical correction of the absorption), the structures were solved by either Patterson or direct methods and refined by full-matrix least squares on weighted F^2 values using the SHELX suite of programs[14] integrated in Olex2.[15] Selected bond lengths and angles can also be found in Tables S3−S6 in the Supporting Information. Because of the poor quality of the data and large amount of crystallographic disorder affecting the tmh ligands, a complete resolution of **4** was not possible. Nevertheless, the unit cell (triclinic, $P\bar{1}$, a = 17.2575(9) Å, b = 17.2939(12) Å, c = 22.9502(20) Å, α = 90.778(2)°, β = 99.607(2)°, γ = 113.889(2)°), a partial refinement, and comparison between the experimental X-ray powder diffraction diagrams of **3** and **4** (Figure S1c in the Supporting Information) confirm that both complexes are isostructural. To carry out the XRPD experiments, crystals of **3** and **4** were ground and deposited in the sample holder of a θ:θ Bruker AXS D8 vertical scan diffractometer. The generator was operated at 40 kV and 40 mA. The scans were performed with 4° < 2θ < 20° with t = 2 s and $\Delta 2\theta$ = 0.005°. CCDC 1522191 (**1**), 1522192 (**2**) and 1522190 (**3**) contain the supplementary crystallographic data for this article. These data are provided free of charge by the Cambridge Crystallographic Data Centre.

Physical Measurements. Elemental analyses were carried out at the "Centro de Instrumentación Científica" of the University of Granada on a Fisons-Carlo Erba Model EA 1108 analyzer. FT-IR spectra were recorded with a Bruker Tensor 27 spectrometer using an ATR accessory. Reflectance spectra were recorded on a Varian Cary 5 UV−vis−NIR spectrophotometer equipped with a "Praying Mantis" dispositive specific for the analysis of small amounts of solid samples. Direct (dc) and alternating current (ac) susceptibility measurements were performed with a Quantum Design SQUID MPMS XL-5 device. ac experiments were performed using an oscillating ac field of 3.5 Oe and frequencies ranging from 1 to 1500 Hz. ac magnetic susceptibility measurements in the range 1−10000 Hz were carried out with a Quantum Design Physical Property Measurement System using an oscillating ac field of 5 Oe. The experimental susceptibilities were corrected for the sample holder and diamagnetic contributions. Pellets of the different samples were cut into small pieces and placed in the sample holder to avoid any orientation of the microcrystals by the magnetic field. Low-temperature magnetization measurements were performed by means of a conventional inductive probe in pulsed-magnetic fields. The temperature was reached as low as 0.5 K using a ^{3}He cryostat.[16] Polycrystalline specimens were mounted in a capillary tube made of polyimide. Samples of approximately 20 mg were not fixed within the sample tube, and then they aligned along the magnetic field direction. Subsequently, a magnetic field was applied several times until the orientation effect was saturated and the magnetization curves obtained in further shots were found to be identical.

Computational Methodology. 4f electrons in lanthanide ions are completely localized in their respective metal centers. These electrons feel much stronger crystal-field and spin−orbit coupling effects in comparison to the exchange interaction between the lanthanide centers. This necessitates the preferential consideration of ligand field and spin−orbit coupling effects in polynuclear lanthanide-based complexes. Importantly, minute competition between spin−orbit coupling and ligand field in 4f shells entails the need of correlated post-Hartree−Fock ab initio calculations. Hence, to deduce magnetic properties of polynuclear lanthanide complexes, we have adopted a computational methodology that uses ab initio computations on monolanthanide fragments in conjunction with a model depiction of the exchange between different monolanthanide fragments. Ab initio calculations on the mononuclear lanthanide fragments (on the crystallographic geometries) were carried out by the most viable CASSCF+RASSI-SO+SINGLE_ANISO approach[17,18] as implemented in the MOLCAS 8 suite.[19,20] To understand how the basis set is influencing the results, we have undertaken studies using four different basis sets, as summarized in Table 1.

Table 1. Approaches Used for Our Calculations:

method	basis set
I	ANO-RCC-VDZ for all elements
II	ANO-RCC-VDZP for Dy, O, and N; ANO-RCC-VDZ for remaining elements
III	ANO-RCC-VTZP for Dy; ANO-RCC-VDZ for remaining elements
IV	ANO-RCC-VQZP for Dy; ANO-RCC-VDZ for remaining elements

DOI: 10.1021/acs.inorgchem.6b03031
Inorg. Chem. 2017, 56, 5594−5610

Scheme 1. Synthesis of Complexes 1−4

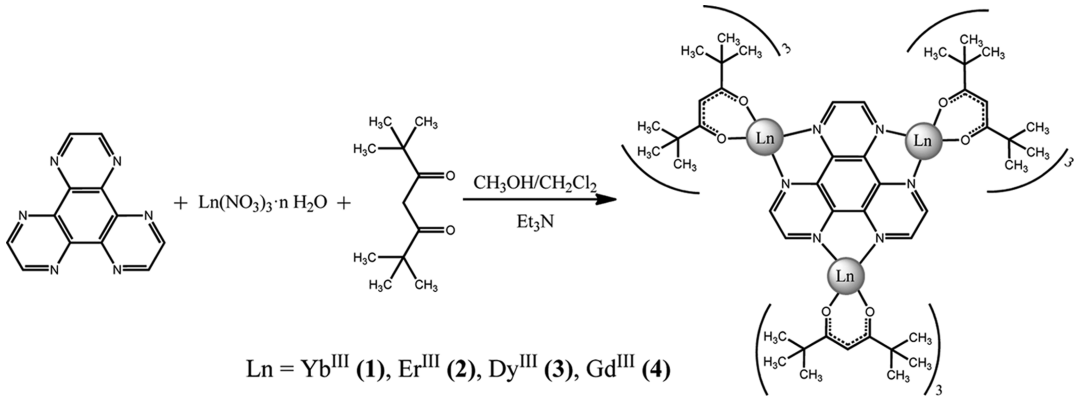

Ln = Yb^{III} **(1)**, Er^{III} **(2)**, Dy^{III} **(3)**, Gd^{III} **(4)**

Specially designed SINGLE_ANISO enables calculations of anisotropic magnetic properties and **g** tensors for the lowest Kramers doublets (KD) of individual mononuclear lanthanide fragments. Hence, magnetic properties of the individual mononuclear lanthanide fragments can be obtained by a parameter-free ab initio approach which accounts for the spin−orbit interaction nonperturbatively. In the mononuclear lanthanide fragment calculations of the CASSCF +RASSI-SO+SINGLE_ANISO approach, two other neighboring Dy^{III} ions (except that on which calculations were to be undertaken) have been computationally substituted by diamagnetic La^{III} ions, as attempted earlier, keeping other parts unaltered. By varying the basis sets from I to IV[19b] we aim to gain insights into the influence of basis sets on the magnetic anisotropy of Dy centers. In order to save disk space, Cholesky decomposition possessing a threshold of 0.2×10^{-7} has been incorporated for our calculations.[22] Within the CASSCF approach, spin-free wave functions and respective energies have been estimated. In our calculations on Dy mononuclear fragment calculations of the Dy_3 polynuclear complex, an active space of the CASSCF[23] method was constructed considering nine electrons in seven 4f orbitals. Further, here in the RASSI-SO[24] step, we have considered only 21 roots, as it has been found to be robust for computing the **g** tensors for Dy^{III} ions.[25] The resultant spin−orbit multiplet can be further used to estimate local magnetic properties via the SINGLE_ANISO[26] approach. Magnetic exchange interactions, exchange spectra and all other magnetic properties of the Dy_3 trinuclear complex have been deduced within the POLY_ANISO[27] routine on the basis of the ab initio results of individual metal fragments.[28]

As expected, upon increasing the basis sets from method I to method II, single-ion energy barriers on the individual Dy centers increased significantly. However, moving to higher basis sets (methods III and IV) did not result in substantial changes in the estimated energy barrier. However, in all approaches, KD1 is found to have axial anisotropy for the three Dy centers. Even wave function analyses at the KD1 level for all sites are the same in all four methodologies tested. In all of the approaches, relaxation is found to occur via the KD2 level for all three Dy centers. Considering the largest single-ion barrier in approach II, the largest diagonal CFP B_2^0 (−1.8 to −2.6) was noted for this method. Despite different basis set combinations, all approaches render similar intramolecular (−0.01 cm^{-1})/intermolecular (−0.00001 cm^{-1}) interactions via best simulation of experimental magnetic data. Considering weak coupling among the Dy centers, in all of the approaches, exchange-coupled ground exchange doublets possess g_{zz} values of ∼18.67−21.95. Following the single-ion characteristics, also in the exchange-coupled system, the overall barrier is noted as being the highest within method II. Here, results obtained from methodology IV are discussed predominantly in comparison with other approaches. However, the corresponding tables and figures pertinent to methods I−III are given in Figures S5−S11 and S13−S15 and Tables S8−S16 in the Supporting Information.

RESULTS AND DISCUSSION

Synthesis and X-ray Crystallography. Complexes **1−4** were prepared by mixing a suspension of HAT ligand in a CH_2Cl_2/CH_3OH mixture with Htmh (9 equiv), Et_3N (9 equiv), and the respective Ln^{III} nitrate salts (3 equiv) dissolved in methanol (Scheme 1). The resulting solutions were left to stand and afforded in every case a good crop of single crystals.

All complexes are isostructural and crystallize in the triclinic $P\bar{1}$ space group. In general, the structures consist of trinuclear entities (Figure 1) where each one of the three Ln^{III} centers are coordinated to a N^N-diimine chelating site of the HAT ligand and three deprotonated tmh ligands.

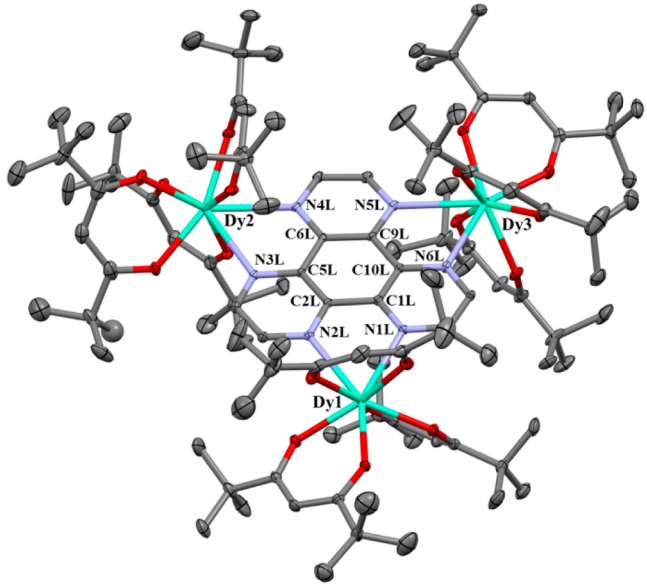

Figure 1. Crystal structure of complex **3**. For the sake of clarity, hydrogen atoms have been omitted and only one component of the disorder involving some of the terminal methyl groups in the tmh ligands is shown. Ellipsoids are drawn at 50% probability.

For **1−3**, the LnN_2O_6 coordination sphere exhibits short $Ln-O_{tmh}$ bond distances, in the range 2.227(2) Å (for the Yb1−O4 bond)−2.342(3) Å (for the Dy1−O1 bond), and longer $Ln-N_{HAT}$ bond distances (in the range 2.256(2) Å for Yb3−N6L and 2.662(3) Å for Dy2−N3L). As expected, the average $Ln-O_{tmh}$ and $Ln-N_{HAT}$ bond distances increase from Yb^{III} to Dy^{III} due to lanthanide contraction. Analysis of the eight-coordinate environments of the metallic centers Ln1−

DOI: 10.1021/acs.inorgchem.6b03031
Inorg. Chem. 2017, 56, 5594−5610

Ln3 by the continuous-shape-measures (CShMs) method[29] revealed that, in the three complexes **1**–**3**, the metal centers Ln1 and Ln3 show a very small deviation parameter (Ln1, 0.499 (**1**), 0.522 (**2**), and 0.569 (**3**); Ln3, 0.543 (**1**), 0.604 (**2**), and 0.694 (**3**)) from the ideal D_{4d} square-antiprismatic geometry, whereas for Ln2 the deviation from this geometry is significantly higher (1.009 (**1**), 1.008 (**2**), and 1.021 (**3**)). Thus, it can be concluded that the coordination environments for Ln1 and Ln3 are very similar to each other and noticeably different for Ln2 (Table S7 in the Supporting Information). The HAT ligand is almost planar with N4L, showing the largest deviation from the mean plane (+0.105 Å (**1**), +0.098 Å (**2**) and +0.088 Å (**3**)) and the three metal centers located out of this plane (Ln1, −0.461 Å (**1**), −0.448 Å (**2**), and −0.462 Å (**3**); Ln2, +0.273 Å (**1**), +0.272 Å (**2**), and +0.273 Å (**3**); Ln3, +0.059 Å (**1**), +0.049 Å (**2**), and +0.046 Å (**3**)). Between the metal centers, the shortest intramolecular distances are found for Ln1···Ln3 (7.908 Å (**1**), 7.946 Å (**2**), 7.998 Å (**3**)) and no relevant short contacts (hydrogen bonds) are found between adjacent trinuclear entities.

Magnetic Properties. The thermal dependence of the dc magnetic susceptibility χ_M of complexes **1**–**4** was measured under an applied magnetic field of 0.1 T in the temperature range 2–300 K (Figure 2). At room temperature, the observed

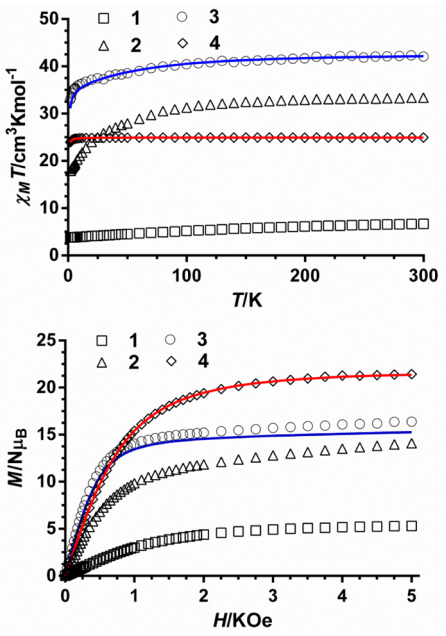

Figure 2. Temperature-dependent $\chi_M T$ plot (top) and field-dependent magnetization plot (bottom) for complexes **1**–**4**. For complex **3** (○), blue lines correspond to ab initio simulations using one possible exchange interaction (J = −0.01 cm^{-1} between three structurally equivalent Dy^{III} centers) and constant intermolecular interaction (zJ) of −0.00001 cm^{-1} (it is noteworthy that all of the J values provided in the graphs correspond to J^{exch} contribution of the total magnetic interaction). For complex **4** (◇), the red lines represent the fitting of the experimental data of **4** to the isotropic Hamiltonian in eq 1.

χ_MT values for **1**–**4** are close to those calculated for the three isolated Ln^{III} ions in the free ion approximation (see Table 2). Upon cooling, the χ_MT product of complexes **1**–**3** decreases slowly at high temperature and more steeply as the temperature decreases to 2 K, which is due to the combined effect of the thermal depopulation of the m_J sublevels of the Ln^{III} ions

Table 2. Direct Current Magnetic Data for the Complexes Studied in This Work

compound	theor $\chi_M T_{300\,K}$ (cm^3 K mol^{-1})[a]	exptl $\chi_M T_{300\,K}$/$\chi_M T_{2\,K}$ (cm^3 K mol^{-1})	theor M_{sat} value (N μ_B)[b]	exptl M_{sat} value (T = 2 K, H = 5 T) (N μ_B)
1	7.71	6.68/3.87	12	5.31
2	34.44	33.34/17.91	27	14.09
3	42.51	42.05/32.99	30	16.38
4	23.63	24.95/23.95	21	21.43

[a] $\chi_M T = \frac{N\beta^2}{3k}\{g_j^2 J(J+1)\}$

[b] $M = NJ\mu_B \quad J = L + S \quad g_J = \frac{3}{2} + \frac{S_T(S_T+1) - L(L+1)}{2J(J+1)}$

arising from the splitting of the ground terms by the ligand field, as well as the possible existence of weak intramolecular antiferromagnetic exchange and/or intermolecular dipolar interactions. The field dependence of the magnetization for complexes **1**–**3** at T = 2 K (Figure 2, bottom) shows a rapid increase of the magnetization at low field (up to ∼1 T) and then increases slowly with the field without reaching saturation at 5 T, which is due to the presence of significant magnetic anisotropy and/or low-lying excited states that are partially (thermal and field induced) populated. The magnetization values at the highest applied dc magnetic field of 5 T are, however, roughly the half of those calculated for three noninteracting Ln^{III} ions (Table 2). This difference can be essentially ascribed to crystal-field effects leading to significant magnetic anisotropy.[30]

When the temperature is lowered, the $\chi_M T$ product for **4** remains almost invariable until ∼10 K and then decreases sharply to reach a value of 23.95 cm^3 K mol^{-1} at 2 K. The decrease in $\chi_M T$ below 10 K is due to the presence of very weak antiferromagnetic interactions between the Gd^{III} ions and/or zero-field splitting (ZFS) effects of the Gd^{3+} ions. The magnetic susceptibility data of **4** were modeled with the following Hamiltonian, where for the sake of simplicity all the magnetic interaction between the Gd^{III} are considered to be equal:

$$\mathbf{H} = J(\mathbf{S}_{Gd1}\mathbf{S}_{Gd2} + \mathbf{S}_{Gd1}\mathbf{S}_{Gd3} + \mathbf{S}_{Gd2}\mathbf{S}_{Gd2}) + \sum_{i=1}^{3} \beta H\cdot(g_i\mathbf{S}) \quad (1)$$

The simultaneous fit of the experimental susceptibility and multitemperature magnetization data (Figure 3, top) with the above Hamiltonian using the full-matrix diagonalization PHI program[31] afforded the following set of parameters: J = −0.001 cm^{-1} and g = 2.054. Although the obtained values are similar to the reported coupling constants for diazine-bridged Gd^{3+} complexes,[32] they should be taken with caution because of (i) the crudeness of the model and (ii) the possible existence of ZFS splitting of the Gd^{3+} ions.

The extracted magnetic parameters clearly indicate that the interaction between the Gd^{III} ions through the HAT tris-bidentate ligand is very weak and most likely antiferromagnetic in nature. Therefore, the Gd_3 complex **4** can be fundamentally considered as a paramagnet. Owing to the fact that, with a few exceptions, isostructural Dy^{III} and Gd^{III} complexes display the same types of magnetic exchange interaction (ferromagnetic or antiferromagnetic), a very weak antiferromagnetic interaction, if any, is expected for the Dy_3 complex **3**.

Magnetocaloric Effect of 4. Gd^{III}-based low-temperature molecular magnetic coolers (MMCs) show an enhanced

DOI: 10.1021/acs.inorgchem.6b03031
Inorg. Chem. 2017, 56, 5594–5610

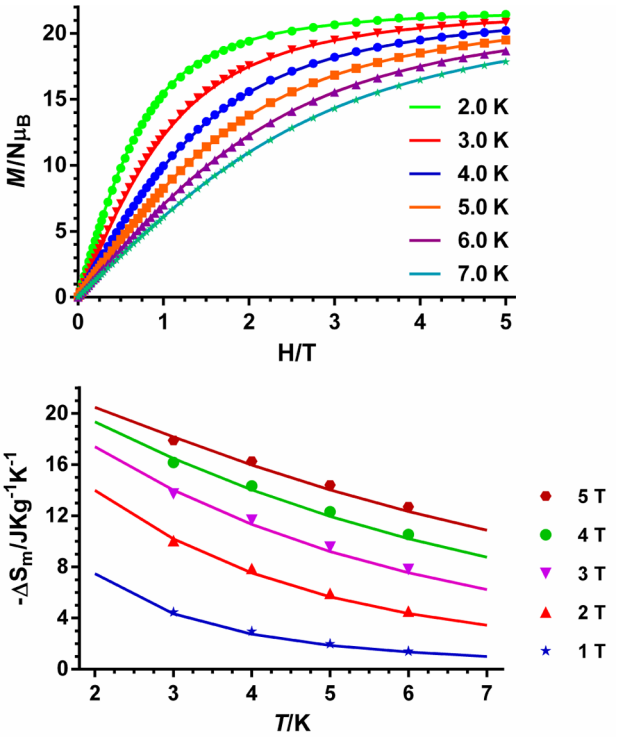

Figure 3. (top) Field dependence of the magnetization plots for **4** between 2 and 7 K and (bottom) magnetic entropy changes ($-\Delta S_m$) simulated using $J = -0.001$ cm^{-1} and $g = 2.045$ (solid lines) and calculated from the experimental magnetization data for **4** from 1 to 5 T and temperatures from 3 to 7 K (points).

magnetocaloric effect (MCE), which is based on the change of magnetic entropy upon application of a magnetic field and can potentially be used for cooling applications via adiabatic demagnetization.[33] We have decided to evaluate the magnetothermal properties of **4** for the following reasons: (i) the antiferromagnetic interactions between the Gd^{3+} ions are very feeble and thus appropriate for a large magnetocaloric effect (MCE), (ii) the Gd^{3+} ion possesses negligible anisotropy due to the absence of orbital contributions, and (iii) Gd^{3+} shows the largest single-ion spin ($S = 7/2$) arising from the $4f^7$ electron configuration. As a result, a considerable MCE is expected for **4**. The magnetic entropy changes ($-\Delta S_m$) that characterize the magnetocaloric properties of **4** can be calculated from the experimental isothermal field-dependent magnetization data (Figure 3, top) by making use of the Maxwell relation:

$$\Delta S_m = (T, \Delta B) = \int_{B_i}^{B_f} \left[\frac{\partial M(T, B)}{dT}\right]_B dB \quad (2)$$

where B_i and B_f are the initial and final applied magnetic fields. The values of $-\Delta S_m$ (Figure 3, bottom) under any field increase, as the temperature decreases from 6 to 3 K. The maximum value of $-\Delta S_m$ achieved is 17.87 J kg^{-1} K^{-1} at $T = 3$ K and applied field change $\Delta B = 5$ T (Figure 3), respectively. In spite of the antiferromagnetic interactions between the Gd^{3+} ions and **4**, there is an important change in $-\Delta S_m$ which is consistent with easy spin polarization at relatively low magnetic field. It is worth noting that we have simulated the MCE for **4** using the magnetic parameters (g and J) extracted from fitting of the magnetization and susceptibility data and the results show that the $-\Delta S_m$ values are almost coincident with those extracted from the integration of the field dependence of the magnetization (Figure 3, top) at different temperatures, thus supporting the $-\Delta S_m$ values extracted from experimental magnetization. The simulated MCE value at 2 K and 5 T (20.46 J kg^{-1} K^{-1}) is only slightly lower than that calculated for the full magnetic entropy content per mole, $nR \ln(2s_{Gd} + 1) = 6.24$, $R = 22.03$ J kg^{-1} K^{-1} for **4**. Moreover, the extracted $-\Delta S_m$ values at 5 T are similar to those found for other Gd_3 complexes but lower than those found for other more magnetic dense Gd_n polynuclear complexes.[34] The results for **4** and other small clusters indicate that these systems could be a good approach for molecular refrigerants.

Magnetization Dynamics in Complexes 1−3. Dynamic ac magnetic susceptibility measurements as a function of temperature and frequency have been performed to determine if complexes **1**−**3** exhibit slow relaxation of the magnetization and SMM behavior.

At zero field, the Yb^{III}(**1**) derivate does not exhibit out-of-phase (χ''_M) signals, due probably to the existence of fast relaxation of the magnetization through quantum tunneling (QTM) and/or to the existence of a too small energy barrier that avoids trapping the magnetization in one of the two equivalent configurations at temperatures above 2 K. For complex **1**, when an external dc field of 1000 G was applied to suppress the QTM, a frequency dependence of the χ''_M signal was observed (Figure 4 and Figure S2 in the Supporting Information) with out-of-phase χ''_M peaks between 2.2 K (800 Hz) and 5.2 K (10000 Hz). The values of the relaxation times (τ) at each temperature were extracted by fitting the frequency dependence of χ''_M at different temperatures to the Debye model. From a fit of these data to an Arrhenius plot, the values of τ_0 and U_{eff} were obtained (Table 3). Almost identical values were obtained from the fit to an Arrhenius plot of the temperatures and frequencies at which the χ''_M signals reach a maximum. The field dependence of τ^{-1} (Figure 4, middle) shows that, at dc fields higher than 0.1 T, τ^{-1} is essentially depicted by the constant parameter C, so that Raman and Orbach processes are dominant. Below 0.1 T, τ^{-1} decreases with an increase in the field, which is due to QTM. The dependence of τ^{-1} on the field has been fitted with eq 3, which considers the field-dependent QTM and direct relaxation processes and also includes a constant C accounting for field-independent Raman and Orbach relaxation processes. The best fit led to the parameters $A = 7310$ s^{-1} K T^4, $B_1 = 4962$ s^{-1}, $B_2 = 5126$ T^{-2}, and $C = 3137$ s^{-1}.

$$\tau^{-1} = ATH^4 + \frac{B_1}{(1 + B_2H^2)} + C \quad (3)$$

In order to know the dominant relaxation process we have fitted the temperature dependence of τ^{-1} with eq 4, which considers the simultaneous presence of Orbach, Raman, QTM, and direct relaxation processes.

$$\tau^{-1} = ATH^4 + \frac{B_1}{(1 + B_2H^2)} + CT^n + \tau_0^{-1} \exp\left(-\frac{U_{eff}}{K_BT}\right) \quad (4)$$

Nevertheless, to avoid overparametrization, the parameters corresponding to QTM (B_1 and B_2) and direct (A) processes were fixed to those previously extracted (see above) from the field dependence of τ^{-1}. The fit shows (Figure 4, bottom) the dominance of a Raman process with a contribution of an Orbach process, which gains weight on increasing temperature. The extracted parameters are given in Table 3. It should be

DOI: 10.1021/acs.inorgchem.6b03031
Inorg. Chem. 2017, 56, 5594−5610

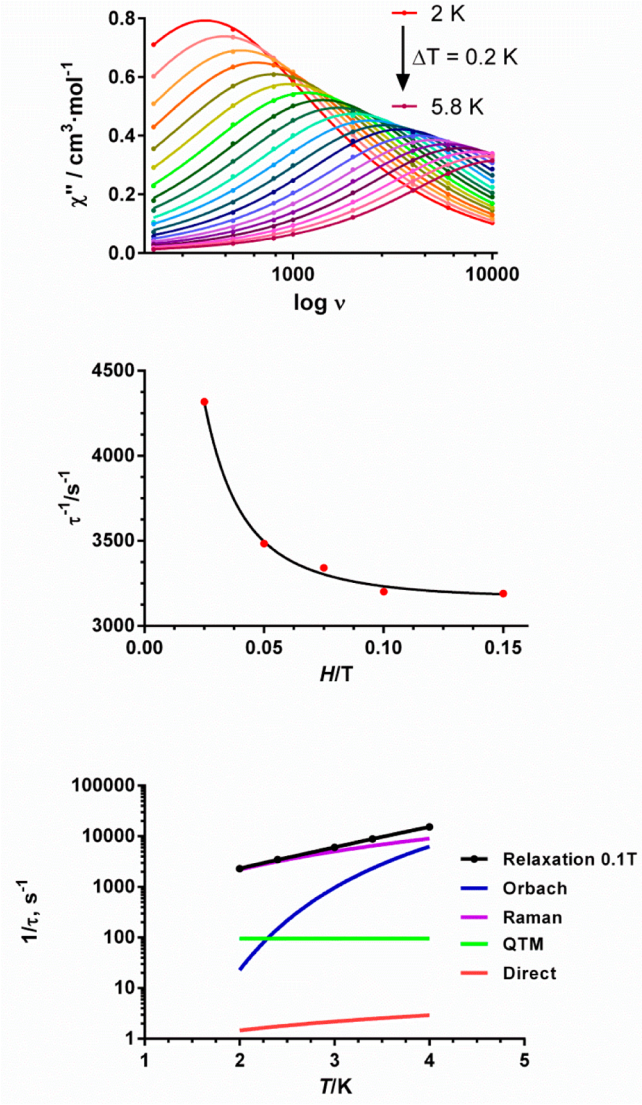

Figure 4. Frequency dependence of the out-of phase ac susceptibility (χ''_M) signal for complex **1** in an applied dc field of 0.1 T (top). Field dependence of τ^{-1} (middle) for complex **1** at T = 2 K (the black line represents the fit to eq 3). Temperature dependence of τ^{-1} for complex **1** (bottom). The black line represents the best fit obtained with eq 4. Purple, blue, green, and red lines represent the contribution of Raman, Orbach, QTM, and direct relaxation processes, respectively.

noted that even though usually n = 9 for Kramers ions,[35] depending on the structure of the levels, n values between 1 and 6 can be considered as reasonable.[36] These results agree with the fact that relaxation of the magnetization in Yb^{III} complexes generally takes place through a Raman process rather than through a thermally activated proces.[37]

The Cole−Cole plot for **1** (Figure S2d in the Supporting Information) in the range of temperature between 2 and 5.6 K shows semicircular shapes with α values (α indicates the width of the distribution of relaxation times with α = 1 corresponding to an infinitely wide distribution of relaxation times and α = 0 to a single relaxation process) ranging from 0.118 to 0.017, which indicate the presence of a narrow distribution of slow relaxation processes in this interval of temperature.

As for **1**, the Er^{III} derivate **2** does not exhibit either of the out-of-phase ac signals unless an external dc field is applied. In the presence of a field of 0.1 T, χ''_M signals appeared in a range of temperature between 2.1 K (4000 Hz) and 2.6 K (10000 Hz), which was indicative of field-induced slow relaxation of the magnetization behavior (Figure 5). An effective energy barrier

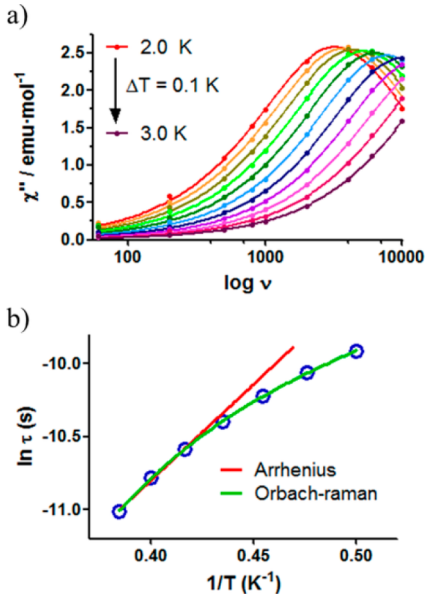

Figure 5. (a) Frequency dependence of the out-of phase ac susceptibility (χ''_M) signal for complex **2** in an applied dc field of 0.1 T. (b) Temperature dependence of the relaxation time τ for complex **2**. The red and green lines represent the best fits of the experimental data to the Arrhenius equation for a thermally activated process and to an Orbach−Raman relaxation process, respectively.

of the magnetization of U_{eff} = 13.2 K and $\tau_0 = 1.05 \times 10^{-7}$ s was calculated from the relaxation times extracted from the fitting of the frequency dependence of the χ''_M data to an Arrhenius law. The deviation of the data in the low-temperature region suggested the existence of a combination of Orbach and Raman relaxation processes of the magnetization. The fit of the temperature dependence of the relaxation times to eq 5 afforded values of U_{eff} = 13.9 K and $\tau_0 = 2.92 \times 10^{-8}$ s (Table 2).

Table 3. U_{eff} and τ_0 Values for Complexes 1−3

	Orbach (H_{dc} = 0.1 T)		several relaxation processes				
compd	U_{eff} (K)	τ_0 (s)	B (s^{-1} K^{-n})	n	U_{eff} (K)	τ_0 (s)	τ_{QTM}
1	21.30	3.7×10^{-7}	534[a]	2.0[a]	22.5[a]	5.7×10^{-7}[a]	
2	13.17	1.1×10^{-7}	1193	5.5	13.86	2.9×10^{-8}	
3	61.6 (SR), 29.6 (FR)	1.2×10^{-6}, 1.3×10^{-6}	0.03	5	69	6.3×10^{-7}	0.05

[a]These parameters were obtained using the values of B_1, B_2 and A extracted from the field dependence of τ^{-1}.

DOI: 10.1021/acs.inorgchem.6b03031
Inorg. Chem. 2017, 56, 5594−5610

$$\tau^{-1} = BT^{n} + \tau_0^{-1} \exp(-U_{eff}/KT) \quad (5)$$

The Cole−Cole diagram for complex **2** (Figure S3d in the Supporting Information) showed a semicircular shape with α values in the range 0.185 (2.0 K)−0.132 (2.5 K) which suggest the existence of several relaxation processes.

In contrast to the previous examples, the Dy^{III} derivative (**3**) showed a clear frequency dependence of the ac susceptibility signals at zero field (Figure S4a in the Supporting Information). Thus, below 30 K, this compound shows two broad maxima in the temperature ranges 16.0 K (2 kHz)−18.0 K (10 kHz) and 6.0 K (2 kHz)−7.6 K (10 kHz) for the slow (SR)- and fast-relaxation (FR) processes, respectively. The broadness of the maxima and the absence of neat peaks below 2 kHz in the χ''_M vs T plot are due to the presence of an overlapping fast quantum tunneling relaxation of the magnetization (QTM), which would be responsible for the typical low-temperature tail (the χ''_M components do not go to 0 below the FR maxima but increase below 5 K). The above facts indicate that compound **3** exhibits slow relaxation of the magnetization and SMM properties under zero applied external magnetic field. Nevertheless, the thermal energy barrier cannot be accurately extracted because the QTM also affects the thermally activated processes. When a small external dc field of 1 kOe (this is the field that induces the slowest relaxation process) was applied to completely or partially remove the QTM relaxation process, two clear peaks appeared at all the used frequencies with maxima in the temperature ranges 6.5 K (60 Hz)−18.0 K (10 kHz) and 3.4 K (60 Hz)−7.6 K (1 kHz) for the slow (SR)- and fast-relaxation (FR) processes, respectively (Figure 6). Moreover, the low tail due to a QTM relaxation process has been almost fully eliminated.

It is worth noting that the observation of several thermally activated relaxation processes is rather common in polynuclear Dy-containing complexes with crystallographically nonequivalent Dy^{3+} and even in cases where all the Dy^{III}centers are crystallographically equivalent. As indicated above, in this complex there exist three crystallographically independent Dy^{III} ions, two of them being very similar (Dy1 and Dy3). Therefore, the fast relaxation process should correspond to Dy2, whereas the slow relaxation process, which gives rise to a broad maximum in the χ''_M vs T plot (Figure 6), should correspond to Dy1 and Dy3. The presence of two relaxation processes can be clearly observed in the Cole−Cole plot (Figure S4c in the Supporting Information). The two relaxation processes were simultaneously fitted with the generalized Debye model, and relaxation times for the FR and SR processes were extracted at different temperatures (Table 3). For these data the Arrhenius plots for the SR and FR processes were constructed and the fit of the high-temperature linear portion of each set of data afforded effective energy barriers, U_{eff}, for a magnetization reversal of 61.6 K (42.5 cm^{-1}) with $\tau_0 = 1.2 \times 10^{-6}$ s and 29.6 K (20.6 cm^{-1}) with $\tau_0 = 1.3 \times 10^{-6}$ s for the SR and FR relaxation processes, respectively. As expected, the Arrhenius plots constructed from the temperatures and frequencies of the maxima observed for χ''_M lead to similar U_{eff} and τ_0 values. The relatively high pre-exponential factors, τ_0, extracted for both relaxation processes could indicate that the QTM has not been fully suppressed. It is well-known that dipole−dipole interactions and hyperfine interactions can favor QTM. In view of this, we decide to magnetically dilute the compound by cocrystallization with an isostructural Y^{3+} diamagnetic species in a Y/Dy molar ratio of 1/10. However, all attempts to obtain the isostructural diluted complexes failed. The relaxation times at low temperature deviate from linearity, which could be due to the existence of relaxation processes other than the thermally activated Orbach process, such as QTM and Raman. In light of this, we decided to fit the data to the equation

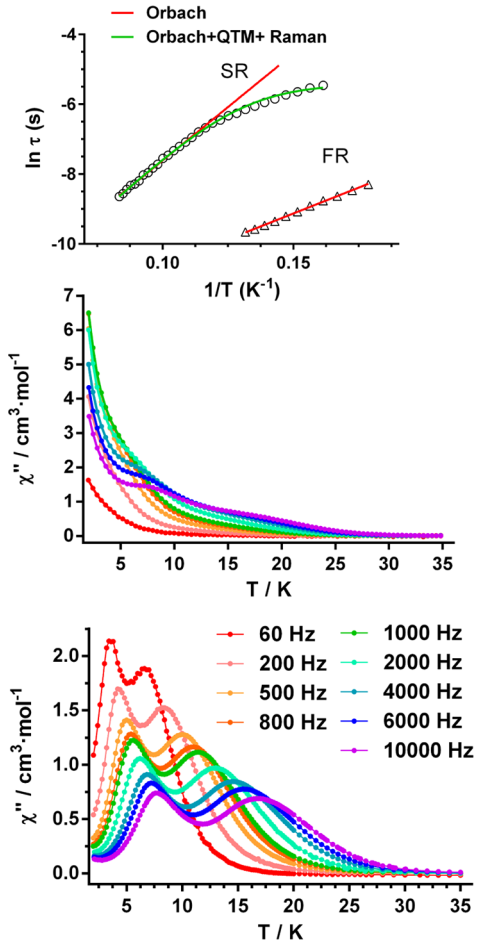

Figure 6. Temperature dependence of the out-of-phase χ_M'' ac signals under zero dc field (middle) and 1000 Oe (bottom) for **3**. Arrhenius plots of relaxation times for the SR and FR of **3** under 1 kOe (top). Red and green solid lines represent the best fitting of the experimental data to the Arrhenius equation and to the Orbach plus Raman plus QTM relaxation processes, respectively.

$$\tau^{-1} = BT^{n} + \tau_0^{-1} \exp(-U_{eff}/KT) + \tau_{QTM}^{-1} \quad (6)$$

The first term corresponds to the two-phonon Raman process, the second term represents the contribution of the two-phonon Orbach process, and the third term symbolizes the QTM process. The best fit of the experimental data in the above temperature range affords for compound **3** the following parameters: $\tau_0 = [6.3(2)] \times 10^{-7}$ s, $U_{eff} = 69(3)$ K (B_{Raman} = 0.03(4) s^{-1}, $n = 5(2)$), and $\tau_{QTM} = 0.05(2)$ (Table 3).

The fact that this compound exhibits a very much higher thermal energy barrier for reversal of magnetization in comparison to compound **2** should be due to the lack of easy-axis anisotropy in the ground doublet state in this latter complex. This could be justified with the help of the simple oblate−prolate model.[38] In complex **3**, the Dy^{III} ions, which have an oblate electron density distribution, show axial anisotropy in the ground state. In contrast, the isostructural Er^{III} complex possesses a prolate electron density distribution

DOI: 10.1021/acs.inorgchem.6b03031
Inorg. Chem. 2017, 56, 5594−5610

and therefore should exhibit easy-plane anisotropy, which stabilizes a ground state with a low m_J value and prevents the observation of SMM behavior.

To know the electronic structure of the Dy^{3+} ions and the exchange-coupled molecule, the nature of the magnetic exchange interaction between the Dy^{3+} ions, and the relative orientation of the local and main anisotropic axes, detailed ab initio calculations were performed on complex **3**. Calculations were performed only on this compound because it is the only one that exhibited slow relaxation of the magnetization at zero applied dc magnetic field. To deduce the electronic nature and magnetic properties of polynuclear lanthanide complexes, we have adopted a computational methodology in two steps that uses ab initio computations on mononuclear Dy^{III} fragments in conjunction with a model depiction of the exchange between different mononuclear Dy^{III} fragments. In the first step, we have adopted CASSCF+RASSI-SO+SINGLE_ANISO[17,18] methodology to estimate local electronic and magnetic properties of the individual mononuclear Dy^{III} fragmented centers, considering intermolecular interactions as -0.00001 cm^{-1} (within SINGLE_ANISO approach).[17] In the second step, the POLY_ANISO[27] routine based on the ab initio results of individual metal fragments was employed to extract the exchange spectrum and all other magnetic properties of complex **3**. Subsequent information can be utilized to illustrate the magnetization dynamics of the Dy_3 complex using the magnetic axiality[28] concept.

Ab Initio Calculations on Dy^{III} Mononuclear Fragments. The computed electronic and magnetic properties of the three individual Dy^{III} free ions in the Dy_3 complex implies the axial nature of the local **g** tensors in the ground Kramers doublet (KD) of the ground $^6H_{15/2}$ multiplet (see Table 4 and Tables S8−S12 in the Supporting Information). Within approach IV, the ground state (GS) KD (KD1) is associated with a large g_{zz} value (19.07, 18.75, and 19.21 for Dy1, Dy2, and Dy3 sites, respectively; see Table 4 and Table S12). This reveals the presence of large magnetic moment approaching toward that expected for a pure $|\pm M_J\rangle$ = 15/2 state of g_{zz}= 20, with very small transverse components along the main anisotropy axes (a yellow dashed line represents the KD1-g_{zz} alignment). As indicated above, continuous SHAPE measurement (CShM) analysis shows two different kinds of Dy^{III} sites. This is evident from the deviation values of 0.57, 1.02, and 0.70 for Dy1, Dy2, and Dy3 sites, respectively, against idealized square-antiprismatic geometry. The greater distortion around the Dy2 center is well reflected by the corresponding smaller g_{zz} value and larger transverse anisotropy in KD1 in approach IV (see Table 4 and Table S12). In all other approaches (methods I−III), KD1 turns out to possess nearly axial anisotropy (see Tables S8−S11). Additionally, larger geometrical distortion around the Dy2 site is also replicated in these methods (see Tables S8−S11).

Table 4. Computed g Tensors, Energy Spectra, Tilting Angles (θ) of the Main Anisotropy Axes of the First Excited (ES1) KD with Respect to the Ground State (GS) KD Employing Methodology IV, and Angles of the Main Anisotropy Axis of GS with the Dy3 Plane (δ) of the Three Individual Dy^{III} Fragments in 3

site	KD	g_{xx}	g_{yy}	g_{zz}	energy (cm^{-1})	θ (deg)	δ (deg)
Dy1	GS	0.09	0.19	19.07	0.00		58.85
	ES1	1.02	2.00	14.93	92.66	51.49	
Dy2	GS	0.12	0.45	18.75	0.00		92.38
	ES1	0.18	0.67	16.66	47.79	25.60	
Dy3	GS	0.10	0.22	19.21	0.00		75.55
	ES1	2.11	5.47	12.84	107.29	46.08	

The calculated directions of the principal anisotropy axis (g_{zz}) on the three Dy^{III} sites employing approach IV has been represented by yellow dashed lines in Figure 7 (corresponding orientations employing other methodologies are shown in Figures S5−S7 in the Supporting Information). The anisotropy axes for Dy1, Dy2, and Dy3 ions form angles with the Dy_3 plane of 58.85, 92.38, and 75.55°, respectively, within approach IV. Similarly, in other methods as well, the KD1-g_{zz} is found to orient ∼60−90° with respect to the Dy3 plane for all three Dy centers (see Table 4 and Table S8 in the Supporting Information). Consequently, the magnetization vectors of the ground KDs do not compensate and the ground state, at variance with other previously reported Dy_3 triangles where the anisotropy axes are coplanar and form a 120° angle, has a net magnetic moment and is paramagnetic. This agrees well with the high value of $\chi_M T$ at 2 K and the absence of an S shape in the low-field magnetization data.

The first excited KD (KD2) possesses substantial transverse anisotropy in all three Dy sites with g_{zz} in the range 14−17 for all four methodologies. In all of the approaches, KD2-g_{zz} orients at a greater angle with respect to KD1-g_{zz} for all three sites (see Table 4 and Table S8 in the Supporting Information). This provokes relaxation via KD2, outlining calculated energy barriers for magnetization reorientation (U_{cal}) as 92.66, 47.79, and 107.29 cm^{-1} for Dy1, Dy2, and Dy3 sites, respectively, employing method IV. Similarly, U_{cal} turns out to be 73.15/34.96/81.92, 131.05/63.25/146.68, and 83.71/40.29/102.33 cm^{-1} in Dy1/Dy2/Dy3 centers employing methods I−III, respectively (see Table 4 and Table S8 in the Supporting Information and Figure 7 and Figures S5−S11 in the Supporting Information). This again confirms the existence of two magnetically different Dy^{III} centers owing to the two different ranges of relaxation barriers (35−60 and 70−150 cm^{-1}). Hence, on the basis of single ion analysis, the complex is expected to show two types of relaxation, which corroborates the two different U_{eff} energy barriers observed experimentally (20.57 and 42.51 cm^{-1}). The computed energy barriers are noted to be larger than those extracted from the experimental magnetic data. These differences can be attributed to the inadequate data in the high-temperature/high-frequency region, which leads to underestimation of the slope of ln τ vs T^{-1}. In addition, this discrepancy can also be ascribed to the limitations of the SINGLE_ANISO routine, which does not consider QTM relaxation.[21,39] Moreover, this corresponds to a preponderance of other contributions of magnetization relaxations in comparison to the Orbach process. Hence, the experimentally observed U_{eff} could not achieve the expected pure Orbach relaxation parthway by the first excited energy multiplet,[39] due essentially to the presence of QTM. The directions of the ground state g_{zz} axis on the three Dy^{III} sites are not parallel to each other and are found to be tilted with Dy1/Dy2, Dy1/Dy3, and Dy2/Dy3 angles of 33.53, 37.85, and 7.20° employing method IV. The tilting is found to be 30.98/39.85/4.34, 41.81/34.67/13.25, 28.35/32.15/4.20, and 33.53/37.85/7.20° with respect to Dy1/Dy2, Dy1/Dy3, and Dy2/Dy3 for methods I−III, respectively. The g_z value of the highest energy KD approaches that expected for a pure $|\pm M_J\rangle$ = 15/2 state (in

DOI: 10.1021/acs.inorgchem.6b03031
Inorg. Chem. 2017, 56, 5594−5610

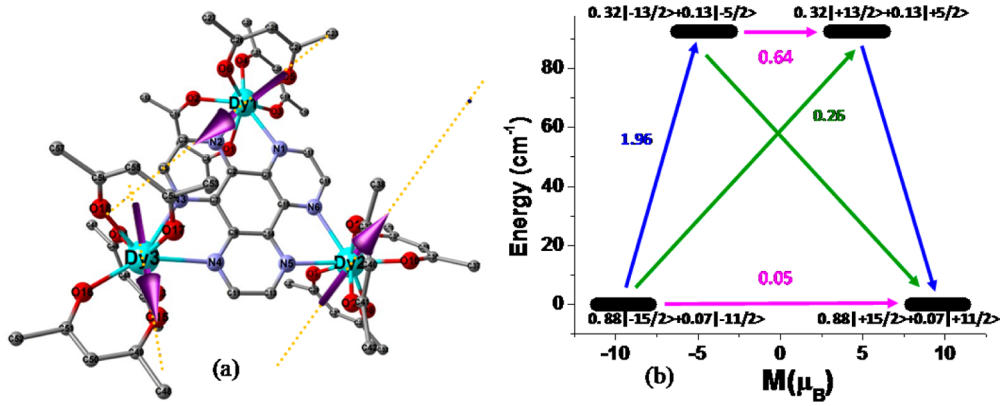

Figure 7. Main magnetic anisotropy axes of the Dy^{III} ions (dashed yellow lines) and orientation of the local magnetic moments (magnetization) in the ground exchange doublet state (purple arrows) (left) and ab initio SINGLE_ANISO computed magnetization blocking barrier for the Dy1 site in the Dy_3 complex (right) employing methodology IV. The *x* axis indicates the magnetic moment of each state along the main magnetic axis of the Dy_3 complex, while the *y* axis denotes the energy of the respective states. The thick black lines indicate the Kramers doublets as a function of their magnetic moment along the main anisotropy axis. The blue and green lines indicate spin−phonon transition (direct/Orbach/Raman) processes. The blue lines additionally represent the most plausible relaxation pathway for the Dy_3 complex. The pink lines correspond to the direct QTM/TA-QTM contribution of relaxation between the connecting pairs. The numbers provided at each arrow are the mean absolute value for the corresponding matrix element of the transition magnetic moment of the respective relaxation process.

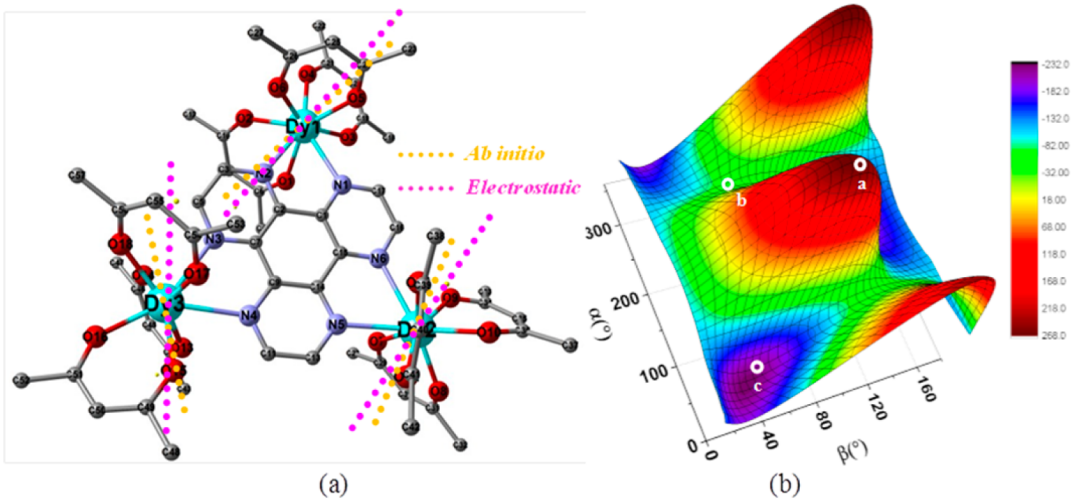

Figure 8. (a) Crystal structure of the Dy_3 complex, where yellow dashed lines show ab initio SINGLE_ANISO computed (employing method I) main anisotropy axes on the three Dy^{III} centers while pink dashed lines indicate electrostatic anisotropy axes obtained from the designed MAGELLAN[37] suite. (b) Electrostatic energy surface constructed considering all possible orientations (α, β) of the Dy1 anisotropy axis in the potential generated by the coordinated charged ligands in the Dy_3 complex. Points a−c indicate maximum, saddle, and minimum points on the electrostatic potential energy surface as governed by the Dy^{III} electron density.

the range ∼18.52−19.82 for all Dy sites irrespective of the methodology considered). This is suggestive of a low symmetric ligand field environment in Dy_3 polynuclear complex[28c] and agrees with the fact that the square-antiprismatic DyO_6N_2 coordination environment of the Dy^{III} ions are rather distorted with large differences between the Dy−O and Dy−N bond distances.

In order to gain deeper insights into the relaxation, we have also plotted the qualitative mechanism of magnetic relaxation for all three individual Dy^{III} centers (see Figure 7 and Figures S5−S11 in the Supporting Information). In the mechanism, KDs have been plotted as per their magnetic moments. Comparatively larger transverse anisotropy for the Dy2 center is well reflected in the KD1 transversal moment matrix elements corresponding to the QTM process (represented by pink lines in Figure 7 and Figures S5−S11) for Dy2 ($\sim 10^{-1}$ μ_B) and Dy1/Dy3 ($\sim 10^{-2}$ μ_B) sites in all of the methodologies. Moreover, our wave function analysis indicates more mixed character of ground KD in the Dy2 center than in the Dy1/Dy3 sites (greater contribution from the ±15/2 multiplet in the Dy1/Dy3 center than in Dy2). Within approach IV, ground $|\pm M_J\rangle$ = 88%$|\pm 15/2\rangle$ + 7%$|\pm 11/2\rangle$, 83%$|\pm 15/2\rangle$ + 8%$|\pm 11/2\rangle$, 88%$|\pm 15/2\rangle$ + 10%$|\pm 11/2\rangle$ for the Dy2, Dy1, and Dy3, centers respectively, and this is replicated in all of the other three approaches (Figure 7 and Figures S5−S11). Additionally, considerable magnetic moment matrix elements (i.e., ∼2 and 0.3 (0.8) μ_B; see Figure 7) corresponding to a spin−phonon transition (direct, Orbach, Raman; denoted by green and blue lines in Figure 7 and Figures S5−S11) instigates relaxation via KD2 for all of the employed methodologies. This was further substantiated by the significant transversal magnetic moment matrix elements within the KD2 levels of reverse magnetization corresponding to the TA-QTM process (i.e 0.2−1.7 μ_B; see the pink lines in Figure 7 and Figures S5−S11). Hence, on the basis

DOI: 10.1021/acs.inorgchem.6b03031
Inorg. Chem. 2017, 56, 5594−5610

of single ion analysis, we can tentatively assign the fast magnetization relaxation to the Dy2 site (smaller energy barrier and larger distortion with respect to ideal geometry), while slow relaxation can be attributed to the Dy1/Dy3 center (larger energy barrier and smaller distortion with respect to the ideal geometry). To further consolidate our point, we have analyzed computed crystal field parameters (CFPs), which reveal negative diagonal and axial (B_2^0) terms in all three centers (see Tables S9−S12). This confirms that the axially elongated D_{4d} coordination environment around all three sites favors the observation of slow relaxation of mechanism in the Dy_3 trinuclear complex. In all three sites, ground ranked (k = 2) extradiagonal (nonaxial; B_2^1, B_2^{-2}) terms are also non-negligible, resulting in mixing of $|\pm M_J\rangle$ levels at the ground KD (competitive nature between diagonal and extradiagonal CFPs). Additionally, the considerably higher ranked extradiagonal (B_4^{-3}) term of Dy2 center ($\sim 10^{-1}$ in contrast to $\sim 10^{-2}$ for Dy1/Dy3 sites) contributes to the detection of slightly larger QTM as well as transverse anisotropy in the ground KD (see Table 4 and Tables S8−S12 in the Supporting Information). As in our earlier attempts,[18a,30b] here as well we have employed an electrostatic model[40] to determine the orientation of the electrostatic anisotropy axis (see Figure 8a). Within approach IV, the deviation is found to be in proximity to the ab initio anisotropy axis (deviations are 10.13, 10.28, and 9.88° for Dy1, Dy2, and Dy3 centers, respectively). The deviations turn out to be 10.44/12.61/11.49, 8.86/4.65/7.73, and 8.48/11.36/8.76° in Dy1/Dy2/Dy3 centers employing methods I−III respectively. This suggests the crucial role of electrostatic charges of the ligands in dictating the orientation of the magnetic anisotropy axis. In our ab initio calculations also, the anisotropy axis has pierced amidst the negative charge field of coordinated β-diketonate ligands in order to minimize the electrostatic repulsive force. We have also deduced the electrostatic energy surface for all three Dy centers by varying the two polar angles α and β, signifying an orientation of the quantization axis of the ground state $|\pm M_J\rangle$ level with respect to the crystal field environment created by the attached ligands. Within approach I, all three energy surfaces contain minimum, maximum, and saddle points (see Figure 8b for the Dy1 site as representative figure where a−c denote maximum, saddle, and minimum points, respectively; for the Dy1 site three maximum and two minimum points were detected, as evident from Figures S12 and S16 for surfaces of Dy2 and Dy3 sites). The maximum points will be detected, given that the anisotropy axis is aligned along the negatively charged β-diketonate ligands. On the other hand, axes passing across the middle of the β-diketonate ligand or along the neutral N-containing ligand will represent minimum or saddle points.

As indicated above, recently a similar Dy^{III}_3 molecule has been reported by Layfield and co-workers.[13] Although some structural parameters for this compound are very similar to those of complex **3**, there are significant differences concerning the DyN_2O_6 coordination sphere, however. Thus, while in Layfield's complex the DyN_2O_6 coordination environments can be described as distorted dodecahedra, in complex **3** the Dy coordination spheres are better described as distorted square antiprisms. These differences, which are more likely due to the different steric properties of the HAT and HAN ligands, are indeed the origin of the differences observed in the U_{eff} values and orientation of the anisotropic axis of the Dy^{III} atoms.

Magnetic Properties of Dy_3 Coupled System. We have also calculated the magnetic susceptibility (see Figure S18 in the Supporting Information) of the whole Dy_3 coupled system as a summation of the individual independent Dy fragments[6c,41] (brown line in Figure S18) using the ab initio approach mentioned above. We have determined the magnetic exchange between the nearest neighbor Dy^{III} ions within the Lines[42] model (as embedded in the designed POLY_ANISO[27] routine), which delineates magnetic interactions between the spin moments of magnetic centers in the absence of spin−orbit coupling by one parameter.[7] Within this model, the following effective Heisenberg Hamiltonian[41] was used:

$$\widehat{H}_{ex} = -\sum_{i=1}^{3} J_i \cdot S_i \cdot S_{i+1} \tag{7}$$

Here, $J_i = J_i^{dipolar} + J_i^{exch}$: i.e., J_i is the total magnetic interaction combination of calculated $J_i^{dipolar}$ and fitted J_i^{exch} parameters. This summation, which depicts the interaction between all neighboring Dy^{III} centers and correlates to the local S = 5/2 spins on Dy^{III} centers in the absence of spin−orbit coupling, has been diagonalized on the basis of the KDs extracted from fragment ab initio calculations.[6c] This approach seems to be viable in this respect, owing to the Ising nature of the ground KD in the three Dy centers with $|\pm M_J\rangle \approx |\pm 15/2\rangle$. On the basis of the computed $2^3 = 8$ exchange eigenstate local excited states on three Dy centers, we have estimated the magnetic properties of the Dy_3 polynuclear complex using the POLY_ANISO routine.[9d] Experimental magnetic data ($\chi_M T$ (T) and M (H)) were nicely reproduced with our simulated magnetic exchange J (see Figure S17 in the Supporting Information for J-model description) value of −0.01 cm^{-1} at intermolecular interaction (zJ)= −0.00001 cm^{-1} (see Figures S19 and S20 in the Supporting Information).

In general, the accuracy of Lines model is accounted for in three limiting cases, with possible exchange between (i) one anisotropic and one isotropic magnetic site (Ising + Heisenberg = Ising exchange), (ii) two anisotropic magnetic sites (Ising exchange), and (iii) two isotropic magnetic sites (Heisenberg exchange). In the present case, owing to the inherent strong anisotropy of the Dy^{III} sites and the simulated negligible magnitude of intramolecular magnetic exchange (in comparison to the large energies of the energy multiplets of individual Dy centers), the Dy−Dy interaction can be assumed to be of Ising type. This can be represented by the equation

$$\widehat{H}_{ex} = -\sum_{i=1}^{3} \tilde{J}_i \tilde{S}_{iz} \tilde{S}_{i+1z} \tag{8}$$

where $\tilde{S}_{iz}$ represents the projection of the pseudospin $\tilde{S}$ = 1/2 representing the KD of the magnetic center Dy_i on the respective local magnetic axis z and also illustrates two states with reverse maximal magnetization on this center (for a very small exchange between the magnetic centers, a very small contribution from connecting states $|+15/2\rangle$ and $|-15/2\rangle$ is expected).[41,43] Concepts based on the Lines model and the aforementioned equation has helped deduction of the equation $\tilde{J}_i = 25 \cos \phi_{i,j+1} J_i$. Here, $\phi_{i,j+1}$ corresponds to the angle between the anisotropy axes on the centers i and i + 1. As $\phi_{i,j+1} \approx 2\pi/3$, $\tilde{J}_i = -12.5 J_{i.}$. For our calculations, it was assumed that $J_{i.} = J(\tilde{J}_i = \tilde{J})$. Now, on the basis of this approximation, we can infer that $\tilde{J}$ will be ferromagnetic type for antiferromagnetic J which leads to ferromagnetic alignment of the pseudospins (local magnetization vectors; see purple arrows in Figure 7 and

DOI: 10.1021/acs.inorgchem.6b03031
Inorg. Chem. 2017, 56, 5594−5610

Figures S5−S7 in the Supporting Information) along the anisotropy axis (see yellow dashed lines in Figure 7 and Figures S5−S7). Notably, the deviations between the main anisotropy axis and local magnetizations of the ground exchange Kramers doublet are found to be minimal: i.e., 0.0015, 0.006, and 0.024° for Dy1, Dy2, and Dy3 centers, respectively, for method IV (see Figure 7). This divergence is noted as 0.004/0.03/0.006, 0.006/0.040/0.008, and 0.042/0.007/0.033°, in Dy1/Dy2/Dy3 centers employing methods I−III, respectively (see Figures S5−S7). The resultant exchange spectrum arising from the interaction of the ground KDs on three Dy sites ($2 \times 2 \times 2 = 8$ exchange states = 3 exchange Kramers doublets) has a narrower span of only ∼0.03−0.06 cm^{-1} and a slightly broader range of low-lying state at ∼0.45−0.47 cm^{-1}. This is due to the very weak Dy−Dy interaction (J^{exch}_{Dy-Dy}) of −0.01 cm^{-1} at a weaker intermolecular exchange of −0.00001 cm^{-1} ($J^{dipolar}$= + 0.0009 cm^{-1}) using all four methodologies (see Table S13 in the Supporting Information).

It is worth noting that, despite the presence of two different types of Dy ions, we have considered only one exchange, as all three ions have close to a square-antiprismatic coordination environment with similar bond lengths and angles around the Dy^{III} ion.[9c] For our calculations, we have also considered local excited energy multiplets of Dy centers, which lead to the observation of exchange Kramers doublets in the Dy_3 triangle due to the overall Kramers nature of the exchange-coupled system (due to the overall odd number of total electrons; overall $|M_J\rangle \geq 15/2 \times 3 = 45/2$).

Understanding the Exchange Spectrum. The resultant exchange Kramers doublets of the exchange spectrum depicted by a single direction of magnetization *Z* (the local magnetization vector along the *z* axis has been represented by purple arrows in Figure 7 and Figures S5−S7 in the Supporting Information) due to the associated negligible transversal magnetization ($g_{xx} \approx g_{yy} \approx 10^{-2}-10^{-6}$). Within method IV, noncompensation of the spins owing to the noncoparallel axes leads to a nonzero magnetic ground state (g_{zz} = 19.31, g_{xx} = 10^{-4}, g_{yy} = 10^{-4}), with the next-higher exchange doublet state lying merely 0.03 cm^{-1} above the ground state possessing a g_z value of 19.09 (see Table 5). This results in a large ground state magnetic moment of $\mu_z = 1/2 g_z \mu_B = 9.66\ \mu_B$: i.e., almost equal to the moment of an individual Dy^{III} center and ascribable to very weakly coupled Dy sites. Employing methodologies I−III, ground state exchange doublets possess g_{zz} values of 18.67, 21.95, and 19.07, respectively (see Tables S14−S16 in the Supporting Information). This invokes that a magnetic moment in the ground exchange doublet similar to that of an individual Dy^{III} site arises due to weakly coupled Dy^{III} centers in Dy_3 complex **3**. Substantial g_{xy} components within ground exchange doublets imply appreciable QTM contribution (∼$10^{-3}\ \mu_B$; see Table 5 and Tables S14−S16). This likely suppresses the magnetization relaxation, and hence a dc magnetic field needs to be applied to provoke relaxation via higher excited exchange multiplets. This justifies the observation of clear maxima only in the presence of an applied field in complex **3**. A small energy difference between the ground and first excited exchange doublet (∼0.03−0.06 cm^{-1}; see Table 5 and Tables S14−S16) and a large magnetic moment of first excited exchange doublet ($\mu_z \approx 9\ \mu_B$) give reasons behind the absence of a prominent S shape in the low-field $M(H)$ curve (see Figure S20 in the Supporting Information).[7a,9e] It should be noted that a similar Dy^{III}_3 molecule recently reported by Layfield and co-workers[13] exhibits *J* values stronger than those found for compound **3**, which can be attributed to the influence of *different* electronic properties of the central bridging ligand in both complexes.

Table 5. Energies (cm^{-1}), Corresponding Tunnel Splitting (Δ_{tun}), and *g* Values (Main Magnetic *g* factors) of the Low-Lying Exchange Doublet State in Dy_3 Complex 3 Employing Method IV[a]

		main value of g tensor		
KD	energy (cm^{-1})			Δ_{tun} (cm^{-1})
1	0.0000	g_{xx}	0.0001	10^{-10}
	0.0000	g_{yy}	0.0007	
		g_{zz}	19.3050	
2	0.0320	g_{xx}	0.0002	10^{-10}
	0.0320	g_{yy}	0.0005	
		g_{zz}	19.0937	
3	0.0662	g_{xx}	0.0002	10^{-10}
	0.0662	g_{yy}	0.0006	
		g_{zz}	25.7320	
4	0.4665	g_{xx}	5×10^{-6}	10^{-10}
	0.4665	g_{yy}	9×10^{-6}	
		g_{zz}	54.1637	
5	47.8209	g_{xx}	8×10^{-5}	10^{-9}
	47.8209	g_{yy}	0.0003	
		g_{zz}	17.6407	
6	47.8635	g_{xx}	0.0050	10^{-10}
	47.8635	g_{yy}	1.6037	
		g_{zz}	16.6021	
7	47.8640	g_{xx}	0.0051	10^{-9}
	47.8640	g_{yy}	1.5397	
		g_{zz}	17.3816	
8	48.1892	g_{xx}	1×10^{-5}	10^{-10}
	48.1892	g_{yy}	0.0001	
		g_{zz}	50.3214	
9	92.6620	g_{xx}	0.0024	10^{-9}
	92.6620	g_{yy}	0.0066	
		g_{zz}	14.3183	
10	92.6875	g_{xx}	0.0030	10^{-9}
	92.6875	g_{yy}	0.0075	
		g_{zz}	14.6749	

[a]We have only summarized the exchange doublets through which eventual magnetization relaxation takes place.

To deduce the structure of the magnetization blockade on the basis of the computed exchange coupled states, we need to appraise the most probable relaxation pathways from the maximum magnetized state of the ground exchange doublet to the time-reversed state with opposite magnetization (see Figure 9, Table 5, and Figures S13−S15 and Tables S14−S16 in the Supporting Information).[28a] As detailed earlier in the single-ion discussion, the relaxation pathway is essentially governed by QTM and spin−phonon transition processes. QTM can occur either within the two energy states of reverse magnetization of a specific doublet or through tunneling by excited exchange multiplets. The former type of QTM process is observed in a Kramers kind of system: i.e., the Dy_3 triangle of our current study. Hence, we need to analyze matrix elements of the transversal magnetic moment for the direct QTM to ascertain the magnetization blockade. We have constructed the exchange spectrum (see Figure 9 and Figures S13−S15) where all the exchange states have been arranged in compliance with their corresponding maximum magnetic moments of the exchange doublets employing all four methodologies. The numbers representing each arrow between any two energy states denote

DOI: 10.1021/acs.inorgchem.6b03031
Inorg. Chem. 2017, 56, 5594−5610

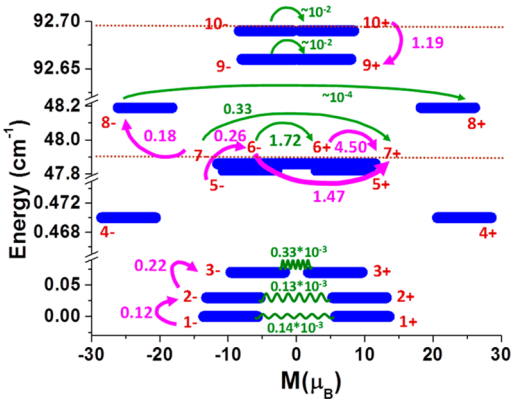

Figure 9. Low-lying exchange spectrum (relative to the energy of the ground state) and position of the magnetization blockade barrier (red dashed line) in Dy_3 complex **3** considering method IV. The bold blue lines indicate exchange states which have been arranged in compliance with the value of their magnetic moments. The green arrows show the same connecting exchange doublet of reverse magnetization and correspond to the direct QTM/TA-QTM contribution to the magnetic relaxation (notably, we have mentioned only $\geq 10^{-3}$ μ_B magnitudes for a clear understanding and better image). The pink arrows infer to the spin−phonon transitions (notably, we have mentioned only $\geq 10^{-1}$ μ_B magnitudes for a clear understanding and better image) between an exchange doublet and its congener higher excited exchange doublets. The numbers near each arrow represent corresponding transversal matrix elements for the transition magnetic moments.

root-mean-square values of matrix elements of magnetic moments (in μ_B). Due to the Kramers nature of the exchange-coupled system, tunnel splitting (Δ_{tun}; between two states of reverse magnetization of a given exchange doublet) within each doublet is negligible ($\leq 10^{-9}$ cm^{-1}) (see Figure 9, Table 5, and Figures S13−S15 and Tables S14−S16). Hence, instead for this system we need to consider the transversal magnetic moment matrix element (of corresponding relaxation pathways) of the ground exchange doublet which is dictated by a Zeeman interaction with a transverse magnetic field. This magnetic moment matrix element within a ground exchange doublet is on the order of $\sim 10^{-3}$ to 10^{-4} μ_B (as represented by green curved/normal arrows in Figure 9 and Figures S13−S15). This $\geq 10^{-3}$ μ_B value promotes relaxation via that particular exchange doublet state ($\leq 10^{-3}$ μ_B opens up a relaxation pathway via higher excited exchange doublets).[28a] On the basis of this criterion, using method IV, a significant transversal magnetic moment matrix element pertinent to the ground exchange doublet QTM is found to be $\sim 10^{-3}$ μ_B. This meets the cutoff value of $\sim 10^{-3}$ μ_B and instigates relaxation within the ground exchange doublet itself.

This entails application of a dc magnetic field to channel relaxation further up via higher excited exchange doublets. Taking into account the considerable matrix element of 1.72 and 0.33 μ_B corresponding to TA-QTM process within the ±6 and ±7 exchange doublets, respectively, a faster relaxation barrier can be outlined as 47.86 cm^{-1} within method IV (see Figure 9 and Table 5). On further movement upward through the excited exchange doublets, a significant matrix element of

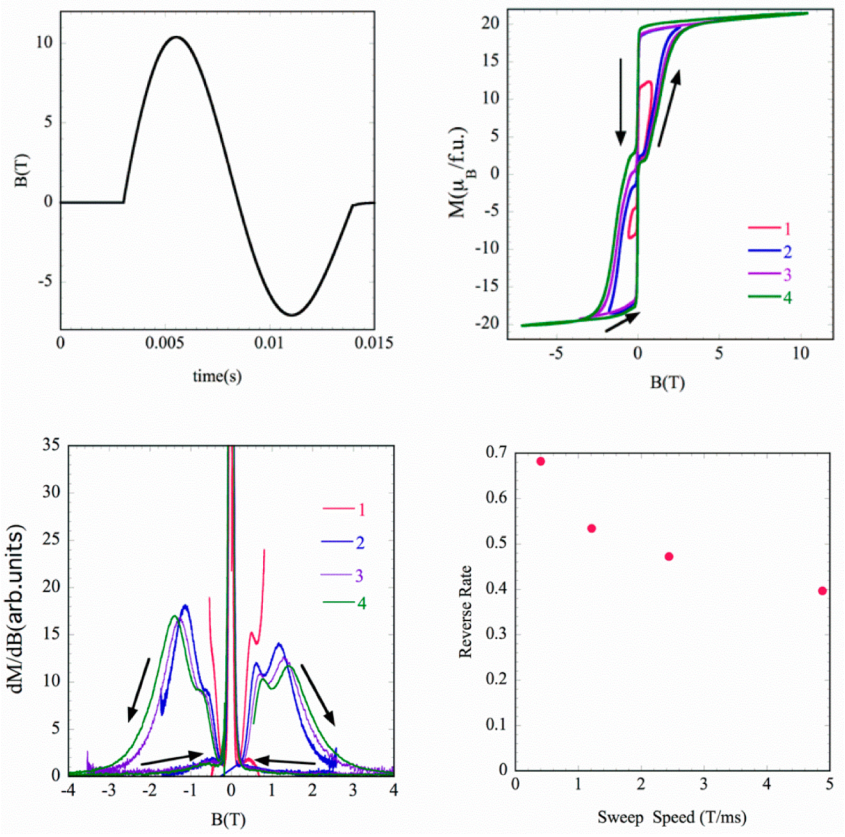

Figure 10. (upper left) Field-scan sequence as a function of time for a maximum field of 10.4 T (4). (upper right) Pulsed-field magnetization curves at maxiumum fields of 0.85 T (1), 2.6 T (2), 5.2 T (3), and 10.4 T (4) for complex **3**. (bottom left) Differential of magnetization for compound **3** measured at 0.4 K. (bottom right) Sweep rate dependence of the reverse rate.

DOI: 10.1021/acs.inorgchem.6b03031
Inorg. Chem. 2017, 56, 5594−5610

$\sim 10^{-2}$ μ_B is detected within the ±9 and ±10 exchange doublets (see Figure 9 and Table 5). Despite a large matrix element between ±9 ($\sim 10^{-2}$ μ_B) states, preferential relaxation via ±10 (TA-QTM pertinent matrix element 10^{-2} μ_B) level can be inferred for the considerable matrix element (1.19 μ_B) for the spin−phonon transition process from −9 to −10 followed by time reversal magnetization (see Figure 9 and Table 5). This postulates a slower U_{cal} value of 92.69 cm^{-1} within approach IV (for approach III, see the Supporting Information). On this note, it is important to pinpoint that exchange between the Dy centers is extremely smaller than the obtained local excitation energies. This suggests a magnetization blockade of the Dy_3 complex to be of single-ion origin (contribution from individual Dy^{III} magnetic sites).[44] Moreover, due to the weak exchange, individual Dy centers are expected to possess independent orientation, which results in fluctuating magnetic field and consequent fast magnetization relaxation.[9a,45] Hence, despite the observation of a multilevel exchange spectrum and the involvement of several relaxation pathways between exchange doublets, the magnetization blockade barrier is principally governed by single-ion properties. It is noteworthy that a blockade barrier has been made without using any fitting parameter other than zJ', which account for intermolecular interactions.[46]

It should be remarked that this compound exhibits a small butterfly shaped hysteresis loop at 2 K using a magnetic field sweep rate of 1.8 mT s^{-1} (Figure S21 in the Supporting Information). The hysteresis lacks appreciable remnant magnetization and coercitive field at zero field. To investigate the magnetization process of the Dy_3 complex, we have also measured the magnetization curve in a full cycle pulsed magnetic field, as shown in Figure 10 (upper left) at 0.4 K.[47] The maximum fields are 0.85, 2.6, 5.2, and 10.4 T, which are hereafter labeled as 1−4, respectively. The magnetic field strength is not symmetric between the positive and the negative directions for the magnet during the pulsing. It should be also noted the sweep rate depends on the maximum field and is highest for 4.

All four magnetization curves in Figure 10 (upper right) show hysteresis loops at low fields and saturations at high fields. For **1**, the field maximum is not enough to reach the saturation. The reduction in the saturation moment to 20 $\mu\beta$/fu is for the powder sample average. There is a double-step structure in the hysteresis which can be clearly observed as two peaks in dM/dB, as shown in Figure 10 (bottom left). In the downward sweep, sharp reversals are found, as shown in Figure S22 in the Supporting Information. There is a fine splitting in the magnetization reversal, as shown in the dM/dB plot in Figure S23 in the Supporting Information.

At zero field before the magnetic field application, we can assume that the low-energy states (1+/−, 2+/−, 3+/−, 4+/−) shown in Figure 9 are equally populated at 0.4 K. Such states give zero magnetization at zero field for the canceling of uncompensated moments. When a magnetic field is applied, the moments antiparallel to the magnetic field direction flip to the parallel direction. It should be noted that the moments are along the local easy axis for the strong anisotropy of Dy. In the Ising limit, states can be expressed by the product of two up/down states at each Dy. Neglecting the small difference in the exchange coupling energy among the three bonds, the states can be classified into four cases such as three-up, two-up and one-down, one-up and two-down, and three-down. The two-up and one-down states can reach the three-up saturated state by a single flip of Dy. However, double site flips and triple site flips are needed in the transitions one-up two-down → three-up and three-down→ three-up, respectively. The Zeeman energy required for reversal of magnetic moments is higher for a larger number of flips, and thus we can expect three steps in the magnetization curve. By using the easy axes for three Dy sites obtained by ab initio calculations, the magnetizations after single, double, and triple spin flips are 0.58, 0.86, and 0.93 of the saturation value of 1. The reduction of the saturation to 0.93 is due to the tilts among the easy axes. We noticed that step heights for the single and double flips are 0.58 and 0.28, while it is only 0.07 for the triple flip. The expected two large steps in the magnetization curve are consistent with the two peak structures observed in experiments. The third small step may appear in the high-field-side tail of the second peak of dM/dB. In Figure 10 (bottom right), we note that the relative ratio between two peaks depends on the sweep rate and the sign of the magnetic field. Such behavior is expected when the reversal mechanism is the mixture of the quantum tunneling and the thermal relaxation. The larger hysteresis in a pulsed field in comparison with that in a steady field is also consistent with the existence of two mechanisms. Namely, the thermal relaxation is suppressed in the fast sweeping pulsed fields and the structure of the level crossing is more highlighted. In this case deviation between the calculated and observed steps heights can occur for the dynamic effect.

Finally, we discuss the sharp reversal around zero field as shown in Figures S22 and S23 in the Supporting Information and Figure 10. Such a sharp change can be mainly attributed to the adiabatic transition at the tunneling gap caused by the avoided level crossing around zero field. A most plausible candidate is the nuclear spin of Dy. In Figure 10 (bottom right) we found a clear sweep rate dependence of the reverse rate defined as the ratio of the magnetization step to the magnetization at 0.1 T. The reduction in the reverse rate for a faster sweeping rate shows the existence of the thermally assisted process. The sizable reverse rate in the fast sweeping limit shows the adiabatic transition. The reverse rate is about 0.4 at 5 T/ms. It is notable that the ratio of the Dy isotopes with nuclear spins is 43%, which is almost comparable with the value of 0.4.

CONCLUSIONS

In conclusion, trinuclear [{Ln(tmh)$_3$}$_3$(μ_3-HAT)] complexes (Ln = Yb (**1**), Er (**2**), Dy (**3**)) have been prepared from the HAT ligand. Dynamic ac magnetic measures reveal that complexes **1** and **2**s how field-induced slow relaxation of the magnetization with U_{eff} values of 21.3 and 13.86 K, respectively. In the case of **3**, SMM behavior is observed at zero field and two different relaxation processes are detected with U_{eff} values of 29.6 K (FR) and 69 K (SR), which are associated with two magnetically different Dy(III) centers in the molecule. Ab initio studies performed on complex **3** indicate that, although the ground state of the three Dy(III) centers is of an Ising type, their anisotropy axes are not coplanar with the HAT ligand. This leads to a paramagnetic ground state and prevents this triangular molecule from behaving as a single-molecule toroic (SMT). Additionally, the magnetocaloric effect of complex **4** was estimated from field-dependence magnetization measurements and a maximum change in magnetic entropy (17.87 J kg^{-1} K^{-1}) was achieved at T = 3 K and ΔB = 5 T.

DOI: 10.1021/acs.inorgchem.6b03031
Inorg. Chem. 2017, 56, 5594−5610

■ ASSOCIATED CONTENT

Supporting Information

The Supporting Information is available free of charge on the ACS Publications website at DOI: 10.1021/acs.inorgchem.6b03031.

Tables and figures as described in the text (PDF)

Accession Codes

CCDC 1522190−1522192 contain the supplementary crystallographic data for this paper. These data can be obtained free of charge via www.ccdc.cam.ac.uk/data_request/cif, or by emailing data_request@ccdc.cam.ac.uk, or by contacting The Cambridge Crystallographic Data Centre, 12, Union Road, Cambridge CB2 1EZ, UK; fax: +44 1223 336033.

■ AUTHOR INFORMATION

Corresponding Authors

*E-mail for J.M.H.: jmherrera@ugr.es.
*E-mail for G.P.: rajaraman@chem.iitb.ac.in.
*E-mail for H.N.: nojiri@imr.tohoku.ac.jp.
*E-mail for E.C.: ecolacio@ugr.es.

ORCID

Juan Manuel Herrera: 0000-0002-9255-227X
Gopalan Rajaraman: 0000-0001-6133-3026

Notes

The authors declare no competing financial interest.

■ ACKNOWLEDGMENTS

I.F.D.-O., J.M.H., and E.C. are thankful for financial support from the Ministerio de Economía y Competitividad (MINECO) for Project CTQ2014-56312-P, the Junta de Andalucía (FQM-195 and the Project of Excellence P11-FQM-7756), and the University of Granada. A part of this work has been carried out at HFLSM, IMR, Tohoku University. I.F.D.-O. also acknowledges support by COLABS. G.R. and T.G. thank the DST-SERB (EMR/2014/00024) for funding.

■ REFERENCES

(1) (a) Sessoli, R.; Gatteschi, D.; Caneschi, A.; Novak, M. A. Magnetic bistability in a metal-ion cluster. *Nature* **1993**, *365*, 141−143. (b) Gatteschi, D.; Sessoli, R.; Villain, J. *Molecular Nanomagnets*; Oxford University Press: Oxford, U.K., 2006.

(2) (a) Milios, C. J.; Vinslava, A.; Wernsdorfer, W.; Moggach, S.; Parsons, S.; Perlepes, S. P.; Christou, G.; Brechim, E. K. A Record Anisotropy Barrier for a Single-Molecule Magnet. *J. Am. Chem. Soc.* **2007**, *129*, 2754−2755. (b) Ako, A. M.; Hewitt, I. J.; Mereacre, V.; Clerac, R.; Wernsdorfer, W.; Anson, C. E.; Powell, A. K. A Ferromagnetically Coupled Mn_{19} Aggregate with a Record S = 83/2 Ground Spin State. *Angew. Chem., Int. Ed.* **2006**, *45*, 4926−4929.

(3) (a) Waldmann, O. A Criterion for the Anisotropy Barrier in Single-Molecule Magnets. *Inorg. Chem.* **2007**, *46*, 10035−10037. (b) Neese, F.; Pantazis, D. A. What is not required to make a single molecule magnet. *Faraday Discuss.* **2011**, *148*, 229−238.

(4) (a) Layfield, R. A.; Murugesu, M. *Lanthanides and Actinides in Molecular Magnetism*; Wiley-VCH: Weinheim, Germany, 2015. (b) Zhang, P.; Guo, Y.; Tang, J. Recent advances in dysprosium-based single molecule magnets: Structural overview and synthetic strategies. *Coord. Chem. Rev.* **2013**, *257*, 1728−1763. (c) Tang, J.; Zhang, P. *Lanthanide Single Molecule Magnets*; Springer-Verlag: Berlin, Heidelberg, 2015. (d) Harriman, K. L. M.; Murugesu, M. An Organolanthanide Building Block Approach to Single-Molecule Magnets. *Acc. Chem. Res.* **2016**, *49*, 1158−1167.

(5) (a) Rinehart, J. D.; Fang, M.; Evans, W. J.; Long, J. R. Strong exchange and magnetic blocking in N_2^{3-} -radical- bridged lanthanide complexes. *Nat. Chem.* **2011**, *3*, 538−542. (b) Chen, Y.; Liu, J.; Ungur, L.; Liu, J.; Li, Q.; Wang, L.; Ni, Z.; Chibotaru, L. F.; Chen, X.; Tong, M. Symmetry-Supported Magnetic Blocking at 20 K in Pentagonal Bipyramidal Dy(III) Single-Ion Magnets. *J. Am. Chem. Soc.* **2016**, *138*, 2829−2837. (c) Gupta, S. K.; Rajeshkumar, T.; Rajaraman, G.; Murugavel, R. An air-stable Dy(III) single-ion magnet with high anisotropy barrier and blocking temperature. *Chem. Sci.* **2016**, *7*, 5181−5191. (d) Liu, J.; Chen, Y.; Jia, J.; Liu, J.; Vieru, V.; Ungur, L.; Chibotaru, L. F.; Lan, Y.; Wernsdorfer, W.; Gao, S.; Chen, X.; Tong, M. A Stable Pentagonal Bipyramidal Dy(III) Single-Ion Magnet with a Record Magnetization Reversal Barrier over 1000 K. *J. Am. Chem. Soc.* **2016**, *138*, 5441−5450. (e) Ding, Y. − S.; Chilton, N. F.; Winpenny, R. E. P.; Zheng, Y. − Z. On Approaching the Limit of Molecular Magnetic Anisotropy: A Near-Perfect Pentagonal Bipyramidal Dysprosium(III) Single-Molecule Magnet. *Angew. Chem., Int. Ed.* **2016**, *55*, 16071−16074.

(6) (a) Tang, J.; Hewitt, I.; Madhu, N. T.; Chastanet, G.; Wernsdorfer, W.; Anson, C. E.; Benelli, C.; Sessoli, R.; Powell, A. K. Dysprosium Triangles Showing Single-Molecule Magnet Behavior of Thermally Excited Spin States. *Angew. Chem., Int. Ed.* **2006**, *45*, 1729−1733. (b) Luzon, J.; Bernot, K.; Hewitt, I.; Anson, C. E.; Powell, A. K.; Sessoli, R. Spin Chirality in a Molecular Dysprosium Triangle: The Archetype of the Noncollinear Ising Model. *Phys. Rev. Lett.* **2008**, *100*, 247205. (c) Chibotaru, L. F.; Ungur, L.; Soncini, A. The Origin of Nonmagnetic Kramers Doublets in the Ground State of Dysprosium Triangles: Evidence for a Toroidal Magnetic Moment. *Angew. Chem., Int. Ed.* **2008**, *47*, 4126−4129.

(7) (a) Ungur, L.; Lin, S.; Tang, J.; Chibotaru, L. F. Single-molecule toroics in Ising-type lanthanide molecular clusters. *Chem. Soc. Rev.* **2014**, *43*, 6894−6905. (b) Gysler, M.; Hallak, F. E.; Ungur, L.; Marx, R.; Hakl, M.; Neugebauer, P.; Rechkemmer, Y.; Lan, Y.; Sheikin, I.; Orlita, M.; Anson, C. E.; Powell, A. K.; Sessoli, R.; Chibotaru, L. F.; Van Slageren, J. Multitechnique investigation of Dy3 - implications for coupled lanthanide clusters. *Chem. Sci.* **2016**, *7*, 4347−4354.

(8) (a) Hewitt, I. J.; Tang, J.; Madhu, N. T.; Anson, C. E.; Lan, Y.; Luzon, J.; Etienne, M.; Sessoli, R.; Powell, A. K. Coupling Dy3 Triangles Enhances Their Slow Magnetic Relaxation. *Angew. Chem., Int. Ed.* **2010**, *49*, 6352−6356. (b) Lin, S.-Y.; Ungur, L.; Soncini, A. Coupling Dy3 Triangles to Maximize the Toroidal Moment. *Angew. Chem., Int. Ed.* **2012**, *51*, 12767−12771. (c) Wang, Y.; Shi, W.; Li, H.; Song, Y.; Fang, L.; Lan, Y.; Powell, A. K.; Wernsdorfer, W.; Ungur, L.; Chibotaru, L.; Shen, M.; Cheng, P. A single-molecule magnet assembly exhibiting a dielectric transition at 470 K. *Chem. Sci.* **2012**, *3*, 3366−3370. (d) Lin, S.; Zhao, L.; Guo, Y.; Zhang, P.; Guo, Y.; Tang, J. Two New Dy3 Triangles with Trinuclear Circular Helicates and Their Single-Molecule Magnet Behavior. *Inorg. Chem.* **2012**, *51*, 10522−10528. (e) Lin, S.; Guo, Y.; Guo, Y.; Zhao, L.; Zhang, P.; Ke, H.; Tang, J. Macrocyclic ligand encapsulating dysprosium triangles: axial ligands perturbed magnetic dynamics. *Chem. Commun.* **2012**, *48*, 6924−6926. (f) Xue, S.; Chen, X.; Zhao, L.; Guo, Y.; Tang, J. Two Bulky-Decorated Triangular Dysprosium Aggregates Conserving Vortex-Spin Structure. *Inorg. Chem.* **2012**, *51*, 13264−13270. (g) Hänninen, M. M.; Mota, A. J.; Aravena, D.; Ruiz, E.; Sillanpää, R.; Camón, A.; Evangelisti, M.; Colacio, E. Two C3-Symmetric Dy3III Complexes with Triple Di-μ-methoxo-μ-phenoxo Bridges, Magnetic Ground State, and Single-Molecule Magnetic Behavior. *Chem. - Eur. J.* **2014**, *20*, 8410−8420.

(9) (a) Das, C.; Vaidya, S.; Gupta, T.; Frost, J. M.; Righi, M.; Brechin, E. K.; Affronte, M.; Rajaraman, G.; Shanmugam, M. Single-Molecule Magnetism, Enhanced Magnetocaloric Effect, and Toroidal Magnetic Moments in a Family of Ln_4 Squares. *Chem. - Eur. J.* **2015**, *21*, 15639−15650. (b) Li, X.; Wu, J.; Tang, J.; Le Guennic, B.; Shi, W.; Cheng, P. A planar triangular Dy_3+Dy_3 single-molecule magnet with a toroidal magnetic moment. *Chem. Commun.* **2016**, *52*, 9570−9573. (c) Zhang, L.; Zhang, P.; Zhao, L.; Wu, J.; Guo, M.; Tang, J. Single-molecule magnet behavior in an octanuclear dysprosium(III) aggregate inherited from helical triangular Dy_3 SMM-building blocks. *Dalton Trans.* **2016**, *45*, 10556−10562. (d) Ungur, L.; Langley, S. K.; Hooper, T. N.; Moubaraki, B.; Brechin, E. K.; Murray, K. S.; Chibotaru, L. F. Net Toroidal Magnetic Moment in the Ground State of a {Dy6}-

DOI: 10.1021/acs.inorgchem.6b03031
Inorg. Chem. 2017, 56, 5594−5610

Triethanolamine Ring. *J. Am. Chem. Soc.* **2012**, *134*, 18554−18557. (e) Guo, P.; Liu, J.; Zhang, Z.; Ungur, L.; Chibotaru, L. F.; Leng, J.; Guo, F.; Tong, M. The First {Dy_4} Single-Molecule Magnet with a Toroidal Magnetic Moment in the Ground State. *Inorg. Chem.* **2012**, *51*, 1233−1235.

(10) Novitchi, G.; Pilet, G.; Ungur, L.; Moshchalkov, V. V.; Wernsdorfer, W.; Chibotaru, L. F.; Luneau, D.; Powell, A. K. Heterometallic Cu^{II}/Dy^{III} 1D chiral polymers: chirogenesis and exchange coupling of toroidal moments in trinuclear Dy_3 single molecule magnets. *Chem. Sci.* **2012**, *3*, 1169−1176.

(11) Sarma, M. S. P.; Czarnik, A. W.Hexadecarboxylative Synthesis of Hexaazatriphenylene. *Synthesis* **1988**, *1988*, 72−73.

(12) (a) Kitagawa, S.; Masaoka, S. Metal complexes of hexaazatriphenylene (hat) and its derivatives—from oligonuclear complexes to coordination polymers. *Coord. Chem. Rev.* **2003**, *246*, 73−88. (b) Shatruk, M.; Chouai, A.; Prosvirin, A. V.; Dunbar, K. R. Structural and magnetic properties of iron(ii) complexes with 1,4,5,8,9,12-hexaazatriphenylene (HAT). *Dalton Trans.* **2005**, 1897−1902. (c) Galán-Mascarós, J. R.; Dunbar, K. R. A microporous framework from a magnetic molecular square: $[Co(HAT)Cl_2]_4$ (HAT = 1,4,5,8,9,11-hexaazatriphenylene). *Chem. Commun.* **2001**, 217−218. (d) Herrera, J. M.; Pope, S. J. A.; Meijer, A. J. H. M.; Easun, T. L.; Adams, H.; Alsindi, W. Z.; Sun, X.; George, M. W.; Faulkner, S.; Ward, M. D. Photophysical and Structural Properties of Cyanoruthenate Complexes of Hexaazatriphenylene. *J. Am. Chem. Soc.* **2007**, *129*, 11491−11504. (e) Herrera, J. M.; Colacio, E.; Mathoniere, C.; Choquesillo-Lazarte, D.; Ward, M. D. Cyanide-bridged tetradecanuclear $Ru^{II}_3M^{II}_{11}$ clusters (M^{II} = Zn^{II} and Cu^{II}) based on the high connectivity building block $[Ru_3(HAT)(CN)_{12}]^{6-}$: structural and photophysical properties. *Chem. Commun.* **2008**, 4460−4462.

(13) Grindell, R.; Vieru, V.; Pugh, T.; Chibotaru, L. F.; Layfield, R. A. Magnetic frustration in a hexaazatrinaphthylene-bridged trimetallic dysprosium single-molecule magnet. *Dalton Trans.* **2016**, *45*, 16556−16560.

(14) Sheldrick, G. M. A short history of SHELX. *Acta Crystallogr., Sect. A: Found. Crystallogr.* **2008**, *64*, 112−122.

(15) Dolomanov, O. V.; Bourhis, L. J.; Gildea, R. J.; Howard, J. A. K.; Puschmann, H. OLEX2: a complete structure solution, refinement and analysis program. *J. Appl. Crystallogr.* **2009**, *42*, 339−341.

(16) Nojiri, H.; Choi, K.; Kitamura, N. Manipulation of the quantum tunneling of nanomagnets by using time-dependent high magnetic fields. *J. Magn. Magn. Mater.* **2007**, *310*, 1468−1472.

(17) (a) Liu, J.; Chen, Y.; Zheng, Y.; Lin, W.; Ungur, L.; Wernsdorfer, W.; Chibotaru, L. F.; Tong, M. Switching the anisotropy barrier of a single-ion magnet by symmetry change from quasi-D_{5h} to quasi-O_h. *Chem. Sci.* **2013**, *4*, 3310−3316. (b) Boulon, M. E.; Cucinotta, G.; Liu, S. S.; Jiang, S. D.; Ungur, L.; Chibotaru, L. F.; Gao, S.; Sessoli, R. Angular-Resolved Magnetometry Beyond Triclinic Crystals: Out-of-Equilibrium Studies of CpErCOT Single-Molecule Magnet. *Chem. - Eur. J.* **2013**, *19*, 13726−13731. (c) Chibotaru, L. F.; Ungur, L. Ab initio calculation of anisotropic magnetic properties of complexes. I. Unique definition of pseudospin Hamiltonians and their derivation. *J. Chem. Phys.* **2012**, *137*, 064112−064122.

(18) (a) Costes, J. P.; Titos-Padilla, S.; Oyarzabal, I.; Gupta, T.; Duhayon, C.; Rajaraman, G.; Colacio, E. Effect of Ligand Substitution around the DyIII on the SMM Properties of Dual-Luminescent Zn−Dy and Zn−Dy−Zn Complexes with Large Anisotropy Energy Barriers: A Combined Theoretical and Experimental Magneto-structural Study. *Inorg. Chem.* **2016**, *55*, 4428−4440. (b) Singh, S. K.; Gupta, T.; Ungur, L.; Rajaraman, G. Magnetic Relaxation in Single-Electron Single-Ion Cerium(III) Magnets: Insights from Ab Initio Calculations. *Chem. - Eur. J.* **2015**, *21*, 13812−13819. (c) Singh, S. K.; Gupta, T.; Rajaraman, G. Magnetic Anisotropy and Mechanism of Magnetic Relaxation in Er(III) Single-Ion Magnets. *Inorg. Chem.* **2014**, *53*, 10835−10845. (d) Gupta, T.; Rajaraman, G. How strongly are the magnetic anisotropy and coordination numbers correlated in lanthanide based molecular magnets? *J. Chem. Sci.* **2014**, *126*, 1569−1579. (e) Gupta, S. K.; Rajeshkumar, T.; Rajaraman, G.; Murugavel, R. An unprecedented zero field neodymium(III) single-ion magnet based on a phosphonic diamide. *Chem. Commun.* **2016**, *52*, 7168−7171. (f) Gupta, S. K.; Rajeshkumar, T.; Rajaraman, G.; Murugavel, R. An air-stable Dy(III) single-ion magnet with high anisotropy barrier and blocking temperature. *Chem. Sci.* **2016**, *7*, 5181−5191. (g) Gregson, M.; Chilton, N. F.; Ariciu, A.; Tuna, F.; Crowe, I. F.; Lewis, W.; Blake, A. J.; Collison, D.; McInnes, E. J. L.; Winpenny, R. E. P.; Liddle, S. T. A monometallic lanthanide bis(methanediide) single molecule magnet with a large energy barrier and complex spin relaxation behaviour. *Chem. Sci.* **2016**, *7*, 155−165. (h) Chilton, N. F.; Goodwin, C. A. P.; Mills, D. P.; Winpenny, R. E. P. The first near-linear bis(amide) f-block complex: a blueprint for a high temperature single molecule magnet. *Chem. Commun.* **2015**, *51*, 101−103. (i) Chilton, N. F. Design Criteria for High-Temperature Single-Molecule Magnets. *Inorg. Chem.* **2015**, *54*, 2097−2099. (j) Upadhyay, A.; Singh, S. K.; Das, C.; Mondol, R.; Langley, S. K.; Murray, K. S.; Rajaraman, G.; Shanmugam, M. Enhancing the effective energy barrier of a Dy(iii) SMM using a bridged diamagnetic Zn(ii) ion. *Chem. Commun.* **2014**, *50*, 8838−8841. (k) Singh, S. K.; Gupta, T.; Shanmugam, M.; Rajaraman, G. Unprecedented magnetic relaxation via the fourth excited state in low-coordinate lanthanide single-ion magnets: a theoretical perspective. *Chem. Commun.* **2014**, *50*, 15513−15516. (l) Pugh, T.; Tuna, F.; Ungur, L.; Collison, D.; McInnes, E. J. L.; Chibotaru, L. F.; Layfield, R. A. Influencing the properties of dysprosium single-molecule magnets with phosphorus donor ligands. *Nat. Commun.* **2015**, *6*, 7492−7500. (m) Ungur, L.; Le Roy, J. J.; Korobkov, I.; Murugesu, M.; Chibotaru, L. F. Fine-tuning the Local Symmetry to Attain Record Blocking Temperature and Magnetic Remanence in a Single-Ion Magnet. *Angew. Chem., Int. Ed.* **2014**, *53*, 4413−4417. (n) Pedersen, K. S.; Ungur, L.; Sigrist, M.; Sundt, A.; Schau-Magnussen, M.; Vieru, V.; Mutka, H.; Rols, S.; Weihe, H.; Waldmann, O.; Chibotaru, L. F.; Bendix, J.; Dreiser, J. Modifying the properties of 4f single-ion magnets by peripheral ligand functionalisation. *Chem. Sci.* **2014**, *5*, 1650−1660. (o) Marx, R.; Moro, F.; Dorfel, M.; Ungur, L.; Waters, M.; Jiang, S. D.; Orlita, M.; Taylor, J.; Frey, W.; Chibotaru, L. F.; van Slageren, J. Spectroscopic determination of crystal field splittings in lanthanide double deckers. *Chem. Sci.* **2014**, *5*, 3287−3293. (p) Le Roy, J. J.; Ungur, L.; Korobkov, I.; Chibotaru, L. F.; Murugesu, M. Coupling Strategies to Enhance Single-Molecule Magnet Properties of Erbium−Cyclooctatetraenyl Complexes. *J. Am. Chem. Soc.* **2014**, *136*, 8003−8010. (q) Venugopal, A.; Tuna, F.; Spaniol, T. P.; Ungur, L.; Chibotaru, L. F.; Okuda, J.; Layfield, R. A. A hydride-ligated dysprosium single-molecule magnet. *Chem. Commun.* **2013**, *49*, 901−903.

(19) (a) Aquilante, F.; Autschbach, J.; Carlson, R. K.; Chibotaru, L. F.; Delcey, M. G.; De Vico, L.; Fdez. Galván, I.; Ferré, N.; Frutos, L. M.; Gagliardi, L.; Garavelli, M.; Giussani, A.; Hoyer, C. E.; Li Manni, G.; Lischka, H.; Ma, D.; Malmqvist, P. Å.; Müller, T.; Nenov, A.; Olivucci, M.; Pedersen, T. B.; Peng, D.; Plasser, F.; Pritchard, B.; Reiher, M.; Rivalta, I.; Schapiro, I.; Segarra-Martí, J.; Stenrup, M.; Truhlar, D. G.; Ungur, L.; Valentini, A.; Vancoillie, S.; Veryazov, V.; Vysotskiy, V. P.; Weingart, O.; Zapata, F.; Lindh, R. Molcas 8: New capabilities for multiconfigurational quantum chemical calculations across the periodic table. *J. Comput. Chem.* **2016**, *37*, 506−541. (b) Aquilante, F.; De Vico, L.; Ferre, N.; Ghigo, G.; Malmqvist, P. A.; Neogrady, P.; Pedersen, T. B.; Pitonak, M.; Reiher, M.; Roos, B. O.; Serrano-Andres, L.; Urban, M.; Veryazov, V.; Lindh, R. MOLCAS 7: The Next Generation. *J. Comput. Chem.* **2010**, *31*, 224−247. (c) Duncan, J. A. MOLCAS 7.2. *J. Am. Chem. Soc.* **2009**, *131*, 2416−2416. (d) Veryazov, V.; Widmark, P. O.; Serrano-Andres, L.; Lindh, R.; Roos, B. O. 2MOLCAS as a development platform for quantum chemistry software. *Int. J. Quantum Chem.* **2004**, *100*, 626−635. (e) Karlstrom, G.; Lindh, R.; Malmqvist, P. A.; Roos, B. O.; Ryde, U.; Veryazov, V.; Widmark, P. O.; Cossi, M.; Schimmelpfennig, B.; Neogrady, P.; Seijo, L. MOLCAS: a program package for computational chemistry. *Comput. Mater. Sci.* **2003**, *28*, 222−239.

(20) Ungur, L.; Chibotaru, L. F. In *Lanthanides and Actinides in Molecular Magnetism*; Wiley-VCH: Weinheim, Germany, 2015; pp 153−184.

DOI: 10.1021/acs.inorgchem.6b03031
Inorg. Chem. 2017, 56, 5594−5610

(21) Langley, S. K.; Ungur, L.; Chilton, N. F.; Moubaraki, B.; Chibotaru, L. F.; Murray, K. S. Single-Molecule Magnetism in a Family of $\{Co^{III}_2Dy^{III}_2\}$ Butterfly Complexes: Effects of Ligand Replacement on the Dynamics of Magnetic Relaxation. *Inorg. Chem.* **2014**, *53*, 4303−4315.
(22) Koch, H.; Sánchez de Merás, A.; Pedersen, T. B. Reduced scaling in electronic structure calculations using Cholesky decompositions. *J. Chem. Phys.* **2003**, *118*, 9481−9484.
(23) Roos, B. O.; Taylor, P. R.; Siegbahn, P. E. M. A complete active space SCF method (CASSCF) using a density matrix formulated super-CI approach. *Chem. Phys.* **1980**, *48*, 157−173.
(24) Roos, B. O.; Malmqvist, P. Relativistic quantum chemistry: the multiconfigurational approach. *Phys. Chem. Chem. Phys.* **2004**, *6*, 2919−2927.
(25) Bernot, K.; Luzon, J.; Bogani, L.; Etienne, M.; Sangregorio, C.; Shanmugam, M.; Caneschi, A.; Sessoli, R.; Gatteschi, D. Magnetic Anisotropy of Dysprosium(III) in a Low-Symmetry Environment: A Theoretical and Experimental Investigation. *J. Am. Chem. Soc.* **2009**, *131*, 5573−5579.
(26) Ungur, L.; Chibotaru, L. F., SINGLE_ANISO module in MOLCAS; http://www.molcas.org/documentation/manual/node95.html.
(27) Ungur, L.; Chibotaru, L. F. *POLY_ANISO program*; KU Leuven, Leuven, Belgium, 2007.
(28) (a) Ungur, L.; Thewissen, M.; Costes, J. P.; Wernsdorfer, W.; Chibotaru, L. F. Interplay of Strongly Anisotropic Metal Ions in Magnetic Blocking of Complexes. *Inorg. Chem.* **2013**, *52*, 6328−6337. (b) Feltham, H. L. C.; Lan, Y.; Klöwer, F.; Ungur, L.; Chibotaru, L. F.; Powell, A. K.; Brooker, S. A Non-sandwiched Macrocyclic Monolanthanide Single-Molecule Magnet: The Key Role of Axiality. *Chem. - Eur. J.* **2011**, *17*, 4362−4365. (c) Ungur, L.; Chibotaru, L. F. Magnetic anisotropy in the excited states of low symmetry lanthanide complexes. *Phys. Chem. Chem. Phys.* **2011**, *13*, 20086−20090.
(29) (a) Alvarez, S.; Alemany, P.; Casanova, D.; Cirera, J.; Llunell, M.; Avnir, D. Shape maps and polyhedral interconversion paths in transition metal chemistry. *Coord. Chem. Rev.* **2005**, *249*, 1693−1708. (b) Cirera, J.; Ruiz, E.; Alvarez, S. Continuous Shape Measures as a Stereochemical Tool in Organometallic Chemistry. *Organometallics* **2005**, *24*, 1556−1562.
(30) (a) Oyarzabal, I.; Ruiz, J.; Ruiz, E.; Aravena, D.; Seco, J. M.; Colacio, E. Increasing the effective energy barrier promoted by the change of a counteranion in a Zn-Dy-Zn SMM: slow relaxation via the second excited state. *Chem. Commun.* **2015**, *51*, 12353−12356. (b) Costes, J. P.; Titos-Padilla, S.; Oyarzabal, I.; Gupta, T.; Duhayon, C.; Rajaraman, G.; Colacio, E. Analysis of the Role of Peripheral Ligands Coordinated to Zn^{II} in Enhancing the Energy Barrier in Luminescent Linear Trinuclear Zn-Dy-Zn Single-Molecule Magnets. *Chem. - Eur. J.* **2015**, *21*, 15785−15796. (c) Feltham, H. L. C.; Lan, Y.; Klöwer, F.; Ungur, L.; Chibotaru, L. F.; Powell, A. K.; Brooker, S. A Non-sandwiched Macrocyclic Monolanthanide Single-Molecule Magnet: The Key Role of Axiality. *Chem. - Eur. J.* **2011**, *17*, 4362−4365. (d) Bi, Y.; Guo, Y.; Zhao, L.; Guo, Y.; Lin, S.; Jiang, S. D.; Tang, J.; Wang, B. W.; Gao, S. Capping Ligand Perturbed Slow Magnetic Relaxation in Dysprosium Single-Ion Magnets. *Chem. - Eur. J.* **2011**, *17*, 12476−12481.
(31) Chilton, N. F.; Anderson, R. P.; Turner, L. D.; Soncini, A.; Murray, K. S. PHI: A powerful new program for the analysis of anisotropic monomeric and exchange-coupled polynuclear d- and f-block complexes. *J. Comput. Chem.* **2013**, *34*, 1164−1175.
(32) Yu, W.; Schramm, F.; Moreno-Pineda, E.; Lan, Y.; Fuhr, O.; Chen, J.; Isshiki, H.; Wernsdorfer, W.; Wulhekel, W.; Ruben, M. Single-molecule magnet behavior in 2,2′-bipyrimidine-bridged dilanthanide complexes. *Beilstein J. Nanotechnol.* **2016**, *7*, 126−137.
(33) (a) Evangelisti, M.; Brechin, E. K. Recipes for enhanced molecular cooling. *Dalton Trans.* **2010**, *39*, 4672−4676. (b) Sharples, J. W.; Collison, D. Coordination compounds and the magnetocaloric effect. *Polyhedron* **2013**, *54*, 91−103. (c) Sessoli, R. Chiling with magnetic molecules. *Angew. Chem., Int. Ed.* **2012**, *51*, 43−45. (d) Luis, F.; Evangelisti, M. In *Molecular Nanomagnet and Related Phenomena*; Gao, S., Ed.; Springer-Verlag: Berlin, Heidelberg, 2014; pp 431−460. (e) Evangelisti, M. In *Molecular Magnets: Physics and Applications*; Bartolomé, J., Luis, F., Fernández, J., Eds.; Springer-Verlag: Berlin, Heidelberg, 2014; pp 365−385. (f) Liu, J.-L.; Chen, Y.-C.; Guo, F.-S.; Tong, M.-L. Recent advances in the design of magnetic molecules for use as cryogenic magnetic coolants. *Coord. Chem. Rev.* **2014**, *281*, 26−49.
(34) Das, S.; Dey, A.; Kundu, S.; Biswas, S.; Narayanan, R. S.; Titos-Padilla, S.; Lorusso, G.; Evangelisti, M.; Colacio, E.; Chandrasekhar, V. Decanuclear Ln_{10} Wheels and Vertex-Shared Spirocyclic Ln_5 Cores: Synthesis, Structure, SMM Behavior, and MCE Properties. *Chem. - Eur. J.* **2015**, *21*, 16955−16967.
(35) Abragam, A.; Bleaney, B. *Electron Paramagnetic Resonance of Transition Ions*; Clarendon Press: Oxford, U.K., 1970.
(36) Shrivastava, K. N. Theory of Spin−Lattice Relaxation. *Phys. Status Solidi B* **1983**, *117*, 437−458.
(37) (a) Liu, J. L.; Yuan, K.; Leng, J. D.; Ungur, L.; Wernsdorfer, W.; Guo, F. S.; Chibotaru, L. F.; Tong, M. L. A Six-Coordinate Ytterbium Complex Exhibiting Easy-Plane Anisotropy and Field-Induced Single-Ion Magnet Behavior. *Inorg. Chem.* **2012**, *51*, 8538−8544. (b) Lin, P. H.; Sun, W. B.; Tian, Y. M.; Yan, P. F.; Ungur, L.; Chibotaru, L. F.; Murugesu, M. Ytterbium can relax slowly too: a field-induced Yb_2 single-molecule magnet. *Dalton Trans.* **2012**, *41*, 12349−12352. (c) Leng, J. D.; Liu, J. L.; Zheng, Y. Z.; Ungur, L.; Chibotaru, L. F.; Guo, F. S.; Tong, M. L. Relaxations in heterolanthanide dinuclear single-molecule magnets. *Chem. Commun.* **2013**, *49*, 158−160. (d) Li, Q. W.; Liu, J. L.; Jia, J. H.; Leng, J. D.; Lin, W. Q.; Chen, Y. C.; Tong, M. L. Fluorescent single-ion magnets: molecular hybrid $(HNEt_3)$-$[Dy_xYb_{1-x}(bpyda)_2]$ (x = 0.135−1). *Dalton Trans.* **2013**, *42*, 11262−11270. (e) Pointillart, F.; Le Guennic, B.; Golhen, S.; Cador, O.; Maury, O. A redox-active luminescent ytterbium based single molecule magnet. *Chem. Commun.* **2013**, *49*, 615−617. (f) Ruiz, J.; Lorusso, G.; Evangelisti, M.; Brechin, E. K.; Pope, S. J.; Colacio, E. Closely-Related $Zn^{II}_2Ln^{III}_2$ Complexes (Ln^{III} = Gd, Yb) with Either Magnetic Refrigerant or Luminescent Single-Molecule Magnet Properties. *Inorg. Chem.* **2014**, *53*, 3586−3594. (g) Oyarzabal, I.; Artetxe, B.; Rodríguez-Diéguez, A.; García, J. A.; Seco, J. M.; Colacio, E. A family of acetato-diphenoxo triply bridged dimetallic ZnIIILnIII complexes: SMM behavior and luminescent properties. *Dalton Trans.* **2016**, *45*, 9712−9726.
(38) Rinehart, J. D.; Long, J. R. Exploiting single-ion anisotropy in the design of f-element single-molecule magnets. *Chem. Sci.* **2011**, *2*, 2078−2085.
(39) Langley, S. K.; Le, C.; Ungur, L.; Moubaraki, B.; Abrahams, B. F.; Chibotaru, L. F.; Murray, K. S. Heterometallic 3d−4f Single-Molecule Magnets: Ligand and Metal Ion Influences on the Magnetic Relaxation. *Inorg. Chem.* **2015**, *54*, 3631−3642.
(40) Chilton, N. F.; Collison, D.; McInnes, E. J. L.; Winpenny, R. E. P.; Soncini, A. An electrostatic model for the determination of magnetic anisotropy in dysprosium complexes. *Nat. Commun.* **2013**, *4*, 2551.
(41) Ungur, L.; Van den Heuvel, W.; Chibotaru, L. F. Ab initio investigation of the non-collinear magnetic structure and the lowest magnetic excitations in dysprosium triangles. *New J. Chem.* **2009**, *33*, 1224−1230.
(42) Lines, M. E. Orbital Angular Momentum in the Theory of Paramagnetic Clusters. *J. Chem. Phys.* **1971**, *55*, 2977−2984.
(43) (a) Soncini, A.; Chibotaru, L. F. Toroidal magnetic states in molecular wheels: Interplay between isotropic exchange interactions and local magnetic anisotropy. *Phys. Rev. B: Condens. Matter Mater. Phys.* **2008**, *77*, 220406. (b) Bencini, A.; Gatteschi, D. *EPR of Exchange Coupled Systems*; Springer-Verlag: Berlin, 1990.
(44) Lin, P. H.; Burchell, T. J.; Ungur, L.; Chibotaru, L. F.; Wernsdorfer, W.; Murugesu, M. A Polynuclear Lanthanide Single-Molecule Magnet with a Record Anisotropic Barrier. *Angew. Chem., Int. Ed.* **2009**, *48*, 9489−9492.
(45) Bhunia, A.; Gamer, M. T.; Ungur, L.; Chibotaru, L. F.; Powell, A. K.; Lan, Y.; Roesky, P. W.; Menges, F.; Riehn, C.; Niedner-Schatteburg, G. From a Dy(III) Single Molecule Magnet (SMM) to a

DOI: 10.1021/acs.inorgchem.6b03031
Inorg. Chem. 2017, 56, 5594−5610

Ferromagnetic [Mn(II)Dy(III)Mn(II)] Trinuclear Complex. *Inorg. Chem.* **2012**, *51*, 9589−9597.
(46) Langley, S. K.; Wielechowski, D. P.; Vieru, V.; Chilton, N. F.; Moubaraki, B.; Chibotaru, L. F.; Murray, K. S. The first 4d/4f single-molecule magnet containing a $\{Ru^{III}_2Dy^{III}_2\}$ core. *Chem. Commun.* **2015**, *51*, 2044−2047.
(47) Saito, K.; Miyashita, S. Magnetic Foehn Effect in Adiabatic Transition. *J. Phys. Soc. Jpn.* **2001**, *70*, 3385−3390.

DOI: 10.1021/acs.inorgchem.6b03031
Inorg. Chem. 2017, 56, 5594−5610